

Journal Pre-proof

New insights on the interpretation of the provenance and evolution of the Silurian units in the central Precordillera, Argentina

Jonatan Ariel Arnol, Agustina Cretacotta, Norberto Javier Uriz, Carlos Alberto Cingolani, Miguel Angelo Stipp Basei



PII: S0895-9811(23)00056-1

DOI: <https://doi.org/10.1016/j.jsames.2023.104245>

Reference: SAMES 104245

To appear in: *Journal of South American Earth Sciences*

Received Date: 31 December 2022

Revised Date: 23 January 2023

Accepted Date: 4 February 2023

Please cite this article as: Ariel Arnol, J., Cretacotta, A., Javier Uriz, N., Alberto Cingolani, C., Angelo Stipp Basei, M., New insights on the interpretation of the provenance and evolution of the Silurian units in the central Precordillera, Argentina, *Journal of South American Earth Sciences* (2023), doi: <https://doi.org/10.1016/j.jsames.2023.104245>.

This is a PDF file of an article that has undergone enhancements after acceptance, such as the addition of a cover page and metadata, and formatting for readability, but it is not yet the definitive version of record. This version will undergo additional copyediting, typesetting and review before it is published in its final form, but we are providing this version to give early visibility of the article. Please note that, during the production process, errors may be discovered which could affect the content, and all legal disclaimers that apply to the journal pertain.

© 2023 Published by Elsevier Ltd.

1 NEW INSIGHTS ON THE INTERPRETATION OF THE PROVENANCE AND EVOLUTION
2 OF THE SILURIAN UNITS IN THE CENTRAL PRECORDILLERA, ARGENTINA.

3 Jonatan Ariel ARNOL^(a); Agustina CRETACOTTA^(a); Norberto Javier URIZ^(a); Carlos Alberto
4 CINGOLANI^(a-b); Miguel Angelo STIPP BASEI^(c)

5 Corresponding author: Jonatan Ariel Arnol. E-mail address: arnoljonatan@gmail.com

6 a) División Científica de Geología-, Paseo del Bosque s/n, 1900, Facultad de Ciencias
7 Naturales y Museo, Universidad Nacional de La Plata (UNLP), La Plata, Argentina.

8 b) Centro de Investigaciones Geológicas, CIG (UNLP-CONICET) diag 113 N° 275,
9 Facultad de Ciencias Naturales y Museo, Universidad Nacional de La Plata, La Plata,
10 Argentina.

11 c) Instituto de Geociências, Centro de Pesquisas Geocronológicas (CPGeo), Rua do
12 Lago 562, Universidade de São Paulo, Brazil.

13
14 **ABSTRACT**

15 In the central region of the Precordillera, San Juan Province, Silurian silicoclastic
16 sedimentites of the Los Espejos Formation crop out in the Jáchal River area. To the south of
17 this region, an equivalent unit is recognized in the San Juan River area (Tambolar
18 Formation). Both units present similar lithological characteristics, however, it has not yet
19 been defined if they share source areas of detrital contributions. On the other hand, for the
20 Jáchal River sector, it is proposed to establish if there were changes in the regions from
21 where the sub-basin received sediment contributions during the Devonian, which can be
22 seen reflected in the detrital zircon contribution patterns of the overlying unit (Talacasto
23 Formation). The present work is part of a series of studies tending to determine the nature
24 and provenance of the Silurian-Devonian sequences of the Central Precordillera. On this
25 occasion, detrital zircon patterns of the detrital sources of the Los Espejos Formation are
26 analysed and compared with the information obtained for the Silurian Tambolar Formation

27 (San Juan River area) and the overlying Devonian Talacasto and Punta Negra formations
28 (Jáchal and San Juan rivers areas). To characterize and compare the studied units, different
29 methodologies were applied, namely sedimentary petrography, heavy minerals studies, and
30 morphological and isotopic analyses of detrital zircons. The analysis of thin sections allowed
31 determining textural and compositional parameters. Through the predominance of detrital
32 minerals, it was possible to establish that the studied units are composed of quartzite-type
33 rocks coming from mature areas, with low percentages of lithic components and abundant
34 opaque heavy minerals of the hematite group. The study of heavy minerals, especially
35 morphological and typological parameters of detrital zircons, allowed to establish recycled
36 and plutonic sources as main modes, as well as the changes that occurred during the basin
37 filling dynamics for Silurian and Devonian times. On the other hand, U-Pb isotopic analysis in
38 detrital zircons indicate that the Pampean-Brasiliano orogenic cycle composes the main
39 source of detritus with ages between 511 and 816 Ma. In second place are the
40 Mesoproterozoic ages, represented by the interval from 1000 to 1350 Ma. The youngest
41 detrital ages show a maximum sedimentation age of 478.5 ± 4.4 Ma (Tremadocian),
42 indicating that younger sources of contribution correspond to the Famatinian Orogen. The
43 Kolmogorov-Smirnoff test revealed that the studied Silurian-Devonian units have similar
44 patterns of sedimentary contributions, which suggests that the sources of provenance were
45 common in both regions and remained active throughout the entire time interval, without
46 significant changes.

47

48 Keywords: U-Pb geochronology; Lu-Hf isotopes; detrital zircons provenance; Los Espejos
49 Formation; Cuyania terrane; South West Gondwana.

50

51 1. INTRODUCTION

52 The Paleozoic sequences of the Argentinian Precordillera have been extensively studied
53 from different approaches, mainly sedimentological and paleontological (Arnol et al., 2022
54 and references therein). The pioneering works to the understanding of sedimentary
55 provenance in the area correspond to Loske (1992, 1994 and 1995) and Kury (1993), who
56 approach different methodologies applied to units of the San Juan and Mendoza provinces.
57 However, analysis of sedimentary provenance evolution are still scarce due to the great
58 exposures of sequences that form part of the Precordillera (Keller, 1999). The Precordillera,
59 as a geological province, was divided into three sub-provinces according to their structural
60 and stratigraphic characteristics: Eastern, Central and Western (Baldis, 1970; Baldis et al.,
61 1981; Ortiz and Zambrano, 1981; Fig. 1). Contributions regarding the sedimentary
62 provenance of exposed lower Paleozoic units of the Eastern Precordillera have been
63 provided by Naipauer et al. (2010) and Abre et al. (2012), given the petrographic,
64 geochemical and isotopic information. Through different methodological approaches, the
65 basal unit of the Tucunuco Group (La Chilca Formation) of the Central Precordillera was
66 analyzed by Abre et al. (2012), while the Gualilán Group and the Tambolar Formation were
67 recently studied by Arnol et al. (2020, 2022). Regarding the Western Precordillera, Abre et al.
68 (2012) studied the Ordovician units, while Giunta et al. (2022) recently provided new
69 information of the Ordovician to Devonian units. Finally, in the Mendoza Precordillera,
70 Cingolani et al. (2013) provided U-Pb ages of the Devonian Villavencio Formation, while
71 Wenger et al. (under review) performed a more complete provenance analysis of this unit.
72 This contribution aims to improve the knowledge of the characteristics of the Silurian
73 successions exposed in the Central Precordillera, particularly in the Jáchal River area,
74 combining different methodologies in order to elucidate the evolution of the sedimentary
75 basin, the provenance of the detrital sources and their relationship with the overlying
76 Devonian succession.

77

78 2. GEOLOGICAL SETTING AND STRATIGRAPHY

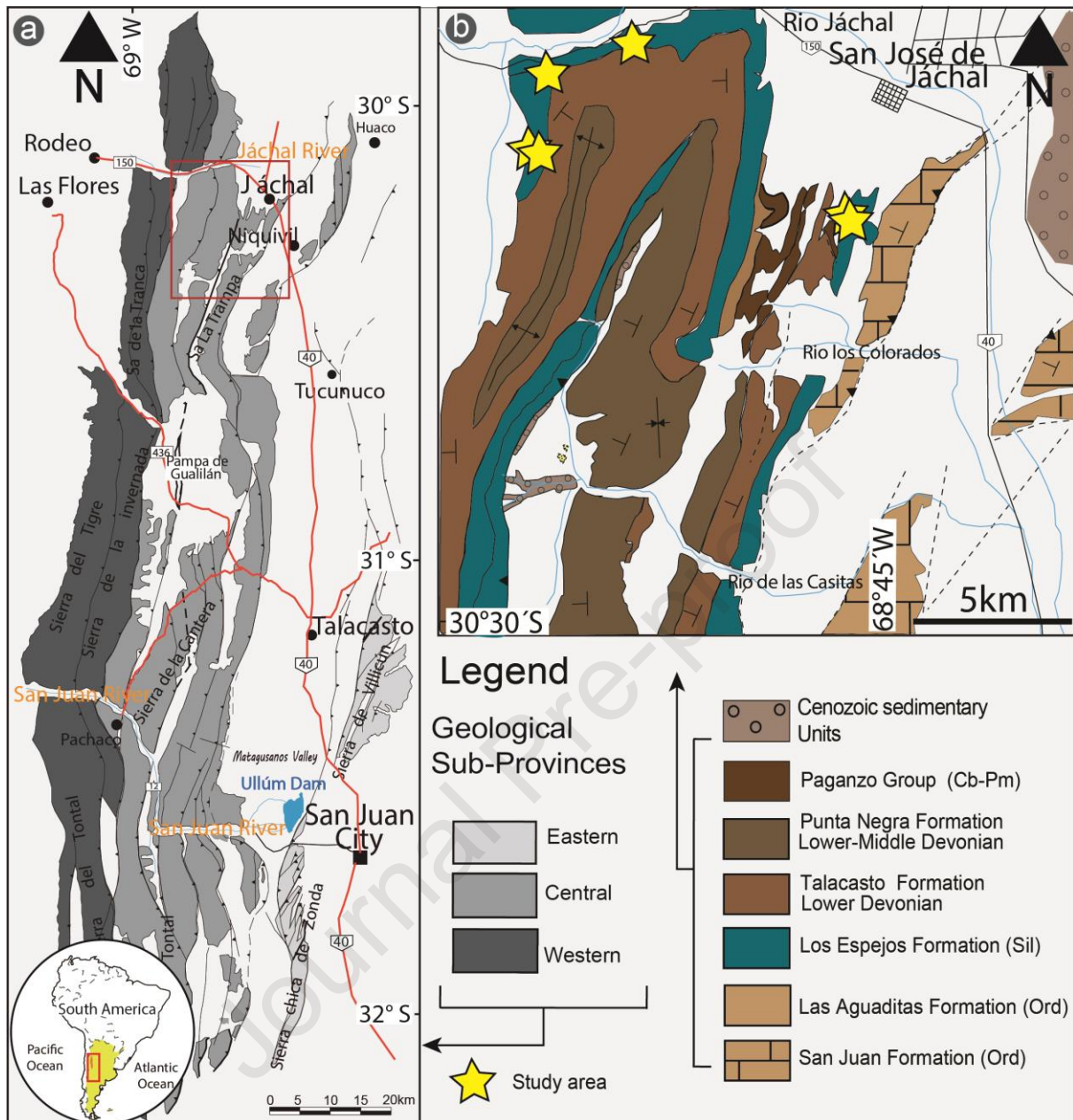
79 The Precordillera is part of the so-called Cuyania terrane (Ramos et al., 1986), for which a
80 Laurentian origin has been attributed (Ramos et al., 1986; Astini et al., 1995; among others)
81 and that would have collided with the western edge of Gondwana during the Middle
82 Ordovician (Vujovich et al., 2004). The collision produced an abrupt increase in the
83 subsidence (drowning) of the platform that was developing at that time. This event was
84 recorded by a gradual transition from shallow carbonate facies to dysoxic and anoxic facies
85 (Astini, 1992; Astini et al., 1995).

86 In the Central Precordillera, Silurian-Devonian silicoclastic marine sequences crop out, which
87 lie on the Ordovician carbonate platform. During Silurian times, the Central Precordillera
88 recorded the Tucunuco Group (Cuerda, 1969), which includes, from base to top, the La
89 Chilca and Los Espejos formations. The Silurian sequence crops out from the north of Jáchal
90 River to Sierra de la Deheza, being its type locality in the Cerro La Chilca (Cuerda, 1965).
91 This group has its maximum thickness to the north of the basin, where it reaches 600 meters
92 and is mainly composed of psamo-pelitic strata (Sánchez et al., 1991), being arranged in
93 erosive unconformity on the carbonate platform.

94 After the drowning of the carbonate platform known as the San Juan Formation, Silurian
95 sedimentites of the La Chilca Formation are exposed in erosive discordance, mainly
96 composed of psamo-pelitic strata (Astini, 1992; Astini et al., 1995). The La Chilca Formation
97 is lithologically characterized by a ca. 20 cm thick basal conglomerate composed of chert
98 clasts, followed by laminated dark beds with abundant graptofauna. Upwards, the deposits
99 become thicker, with a rhythmic deposition, increasing the sand-pelite ratio in the upper part
100 and observing that the sand strata coalesce towards the northern sector of the basin,
101 increasing its thickness (Astini and Maretto, 1996), which does not exceed 200 meters. The
102 temporal range goes from the Hirnantian to the Llandoveryan (Cuerda et al., 1988; Lenz et
103 al., 2003). For its part, the Los Espejos Formation is characterized by the occurrence of a
104 ferruginous basal conglomerate, covered by green and purple shales that alternate with silt
105 up beds, followed by shales and olive-green sandy shales, finely stratified and with the
106 presence of graptolites, tentaculites, brachiopods and trilobites. The sand content increases

107 to the top, forming a coarsening- and thickening-upward strata arrangement. They also
108 contain levels of tabular coquinas of autochthonous or para-autochthonous origin. The unit is
109 usually covered by amalgamated sandstones sequences in the North and Central sections.
110 The shales are strongly bioturbated, recording the *Cruziana* ichnofacies. The maximum
111 thickness reached in the northern sector of the basin (Cerro del Fuerte and Loma de Los
112 Piojos area) is around 500 meters, while towards the south does not exceed 25 meters
113 (Astini and Maretto, 1996; Benedetto et al., 1996).

114 Towards the south, in the San Juan River section, equivalent deposits of the Tambolar
115 Formation (Bracaccini, 1949; Heim, 1952) crop out, being its type section in Portezuelo del
116 Tambolar, on the old road that linked the San Juan and Calingasta localities. For this region,
117 Arnol et al. (2022) highlighted that the unit is characterized by having a high percentage of
118 rounding of its detrital zircons, although the original characteristics are not obliterated. A
119 domain of zircons derived from plutonic sources is observed over the metamorphic ones,
120 where the most representative ages are Neoproterozoic, followed by Mesoproterozoic ages.
121 The presence of Famatinian ages, as well as the low and null proportions of
122 Paleoproterozoic and Archean ages, respectively, are conspicuous for this unit.



123

124 **Figure 1. a)** Tectonic subdivision of the San Juan Precordillera. **b)** Detailed map of the area
 125 studied in this work. Sampling locations represented as yellow stars. Modified from Astini
 126 (1992) and Arnol et al. (2020, 2022).

127

128 3. SAMPLING AND METHODOLOGY

129 The Los Espejos Formation was studied in two different sections, near the San José de
 130 Jáchal locality. In order to obtain relevant information regarding each section, petrographical,

131 morphological (detrital zircon), geochronological (U-Pb) and isotopic (Lu-Hf) studies were
 132 carried out (Table 1).

133 **Table 1** Coordinates and analysis carried out on samples studied in this work.

Sample	Latitud	Longitud	Methodology
16LE12	30°17'49.69"S	68°46'21.49"W	Petrography
16LE13	30°17'49.26"S	68°46'18.76"W	Petrography
16LE22	30°15'30.84"S	68°56'14.79"W	Petrography
16LE25	30°15'35.42"S	68°56'9.32"W	Petrography
16LE26	30°13'11.96"S	68°55'15.77"W	Petrography
16LE29	30°12'35.25"S	68°53'7.95"W	Petrography, Zr morphology, U-Pb and Lu-Hf

134

135

136 *3.1 Petrography*

137 Six thin sections of sandstones were studied under the microscope and quantitatively
 138 analyzed with a Swift-type point counter. Using the traditional method of Gazzi-Dickinson,
 139 400 points were counted (Ingersoll et al., 1984). Classic procedures for petrographic
 140 classification of rocks were followed, applying the schemes proposed by Garzanti (2016).
 141 The ternary diagrams of Dickinson et al (1983) were used for the sedimentary provenance
 142 studies. The results were integrated with data from the same or equivalent units published in
 143 previous works. The populations represented in each triangle include detrital grains, except
 144 for micas, opaque minerals, chlorite, heavy minerals and carbonate grains. Chert was
 145 counted as a sedimentary lithic clast. Petrographic assessment (textural and optical
 146 characteristics of minerals as well as paragenetic associations) allows establishing the
 147 tectonic sedimentary environment using classic discrimination diagrams.

148

149 *3.2 Detrital zircon analysis*

150 Sample 16LE29 was processed by physical methods (crushing, milling, and sieving) to
 151 collect heavy minerals by classical concentration methodologies. The zircon grains were
 152 identified and hand-picked under the binocular microscope (ZEISS Stemi 2000-C model).
 153 Morphological and typological studies on the zircon crystals were carried out with a Scanning
 154 Electron Microscope (JEOL JSM 6360 LV) at the *Museo de La Plata* according to the

155 procedures applied by Gärtner et al. (2013) to determine the main morphological populations
156 and the preliminary provenance of the detrital sources (Dickinson and Gehrels, 2003). The
157 Pupin (1980) classification was used to expand the interpretations of euhedral zircons. The
158 morphological parameters identified on zircons were compared with the data presented by
159 Arnol et al. (2020) and Cretacotta (2022) for Silurian-Devonian sequences of the San Juan
160 Precordillera.

161
162 Selected zircon grains were mounted in epoxy resin and their internal structures were
163 exposed by polishing for cathodoluminescence imagery and dating. The U-Pb and Lu-Hf
164 data were obtained at the Centro de Pesquisas Geocronológicas (CPGeo) of the
165 Universidade de São Paulo, Brazil, with a Thermo Fisher Neptune LA multicollector ICP-MS
166 equipped with a 193 Photon laser system.

167 *3.2.1 U-Pb analysis*

168 Each analysis was composed of 40 sequential measurements (of approx. 1s of integration
169 each) in the ICP-MS "Neptune", 10 with the laser off (to obtain the instrumental blank) and 30
170 under the ablation of the excimer laser "Analyte Excite". 7 isotope signals were measured
171 simultaneously, 4 in Faraday cups (of greater amplitude): ^{206}Pb , ^{208}Pb , ^{232}Th , ^{238}U and 3 in
172 MICs ("Multiple Ion Counters" of greater sensitivity): ^{202}Pb , ^{204}Pb and ^{207}Pb . At the end of
173 each measurement sequence, the mean value of the instrumental blank is immediately
174 subtracted from each of the seven isotope signals. The signal of the isotope ^{235}U is not
175 measured but obtained mathematically, dividing the signal ^{238}U by the relative abundance
176 $238/235$ ($= 137.88$). The participation of Hg (of the carrier gas) in signal ^{204}Pb was discounted
177 by subtracting from it the quotient: signal ^{202}Pb / relative abundance $202/204$ ($= 4.355$). Using
178 the ratios: $^{206}\text{Pb}/^{238}\text{U}$, $^{207}\text{Pb}/^{235}\text{U}$ and $^{208}\text{Pb}/^{232}\text{Th}$ as age estimates and the Stacey-Kramers
179 (1975) formulas, the relative abundances (variables with geological age) were calculated:
180 $206/204$, $207/204$ and $208/204$. The "common Pb" (non-radiogenic) fraction of the isotopes:
181 206 , 207 and 208 is then discounted by subtracting the 204 from each of them multiplied by
182 their respective relative abundance: $206/204$, $207/204$ and $208/204$. Analysis of the GJ-1

183 standard were redone every 10 minutes to correct errors and/or variations in the instrument
184 of subsequent samples. The comparison between tabulated and measured GJ-1 values
185 provides: The (multiplicative) coefficients used to convert the three total signals: Pb (204 +
186 206 + 207 + 208), Th (232) and U (235 + 238) in ppm. The fractionation correction factors of
187 the four ratios: 206/238, 207/235, 207/206 and 208/232 before these were finally used to
188 calculate the (respective) ages. All the LA-ICP-MS U-Pb zircon data are shown in the
189 supplementary material.

190 3.2.2 Lu-Hf analysis

191 Each Lu-Hf analysis consists of 40 sequential measurements performed in the ICP-MS: 10
192 with the laser off (measurement of instrumental blank) and 30 with the laser on (laser
193 ablation on GJ-82C and 91500 standards, or the analyse). Each measurement lasts
194 approximately 1 second. Eight isotopes were measured simultaneously using only Faraday
195 cups: 172, 173, 174, 175, 176, 177, 178, and 180. At the end of each sequence of
196 measurements, the value of the instrumental blank is subtracted from each of the eight
197 isotope signals. Abundance values published by the IUPAC ([https://ciaaw.org/pubs/TICE-](https://ciaaw.org/pubs/TICE-2009.pdf)
198 2009.pdf) were then used to calculate the isotopic ratios between the Yb (172, 173, 174,
199 176), Lu (175, 176), and Hf (176, 177, 178, 180) signals. Signals 172, 173, and (part of) 174
200 were used to calculate the fractionation coefficient of Yb (β_{Yb}) using exponential law. Signals
201 180, 178, 177, and (part of) 174 were used to calculate the fractionation coefficient of Hf
202 (β_{Hf}) also using exponential law. As Lu does not have enough isotopes to allow self-
203 correction, the fractionation coefficient of Lu is assumed to be: $\beta_{Lu} = \beta_{Hf}$. The $^{176}\text{Hf}/^{177}\text{Hf}$
204 ratio can then be readily obtained after subtracting the two interferences: ^{176}Yb (estimated
205 via β_{Yb}) and ^{176}Lu (estimated via β_{Lu}) from the 176 total signal. Before and after the
206 analysis, blanks and zircon standards GJ-82C and 91500 were measured. The analyses of
207 the standards were repeated at regular intervals in order to correct the errors and/or
208 variations of the equipment in the following measurements. Liu et al. (2010) reported an
209 $^{176}\text{Hf}/^{177}\text{Hf}$ value of 0.282015 ± 0.000025 for the GJ-82C standard, while Woodhead and

210 Hergt (2005) reported an $^{176}\text{Hf}/^{177}\text{Hf}$ value of 0.282306 ± 0.000006 for the 91500 standard.
211 The $^{176}\text{Hf}/^{177}\text{Hf}$ values obtained for these standards at the CPGeo during the analysis
212 period were 0.282015 ± 0.000025 (GJ-82C) and 0.282054 ± 0.000020 (91500). The
213 parameters ϵHf and T_{DM} are then finally calculated using the formulas of Yang et al. (2007).
214 All the LA-ICP-MS Lu-Hf zircon data are shown in the supplementary material.

215 **4. RESULTS**

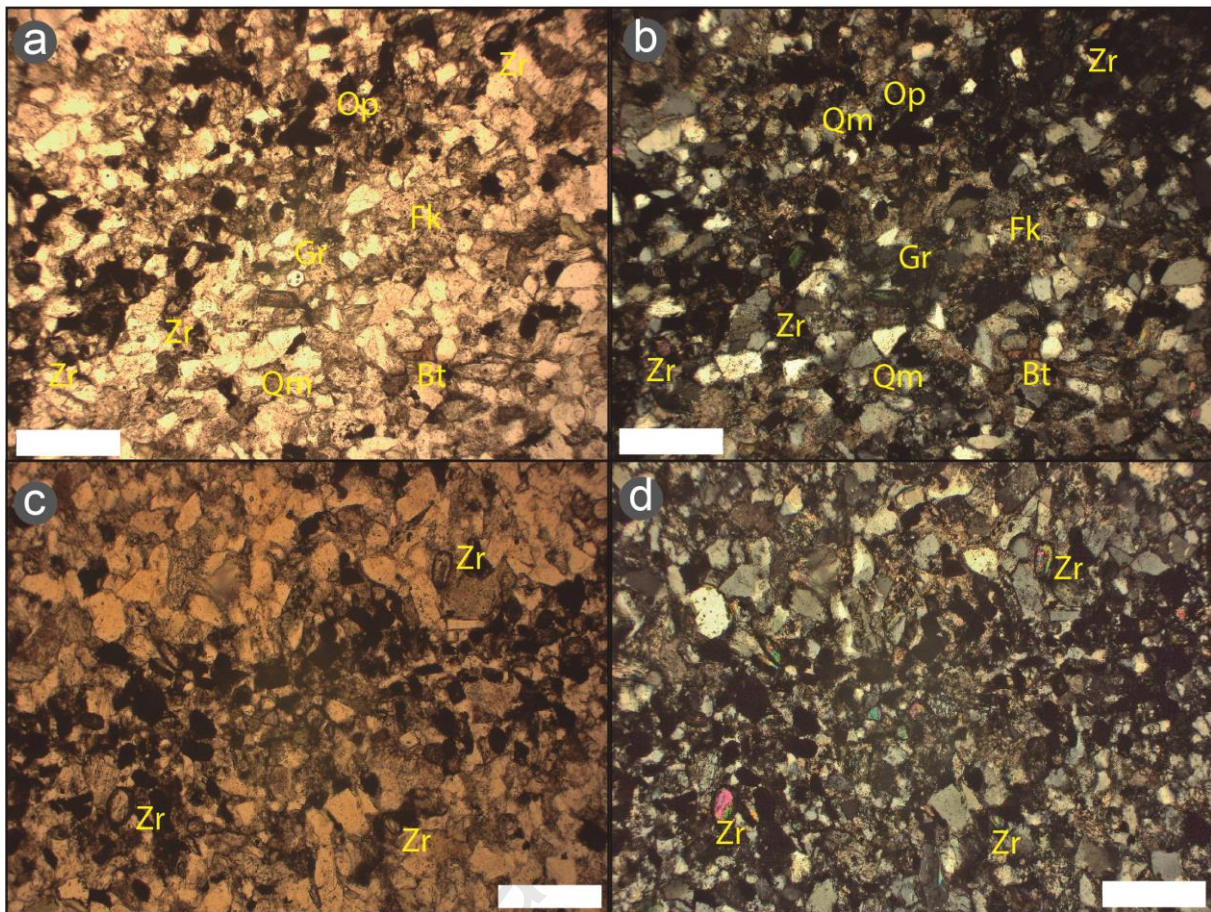
216

217 *4.1 Petrography*

218 Given that the analyzed samples show similarities according to their petrographic
219 characteristics, a general description is provided for characterize them.

220 The Los Espejos Formation is represented by medium-grained rocks, with a moderate
221 selection of its components inferred from their subangular to angular edges. These rocks are
222 mainly composed of monocrystalline quartz grains, mostly with undulose extinction, with
223 sutured edges between crystals, triple junctions and, in some cases, with embayments.
224 Polycrystalline quartz is of small size and is found in low proportion, making it difficult to
225 identify. Plagioclase constitutes a secondary detrital component, with subangular crystals
226 slightly altered to carbonates at its edges and showing the classic polysynthetic twinning.
227 Potassium feldspar is totally altered to carbonates forming a pseudomatrix. Micas are scarce.
228 Muscovite appears as disperse detritus, while biotite occupy holes left by other minerals and
229 is sometimes deformed. Accessory minerals include small concentrations of magnetite and
230 hematite forming mantles (Fig. 2). In the opaque minerals concentrations, abundant
231 translucent heavy minerals are present, with zircon, apatite and rutile as the main minerals.
232 The cement is composed by illitic clay on the one hand, surrounding the crystals of the
233 aforementioned minerals and forming an incomplete ring, while on the other hand, carbonate
234 cement is observed replacing feldspars, both partially (K-feldspar and plagioclase) and
235 completely (K-feldspar). It is defined as a macrosparitic cement that in some sectors behaves
236 like a poikilotropic. A third type of cement is composed of a light brownish sericite filling the
237 rock pores.

238

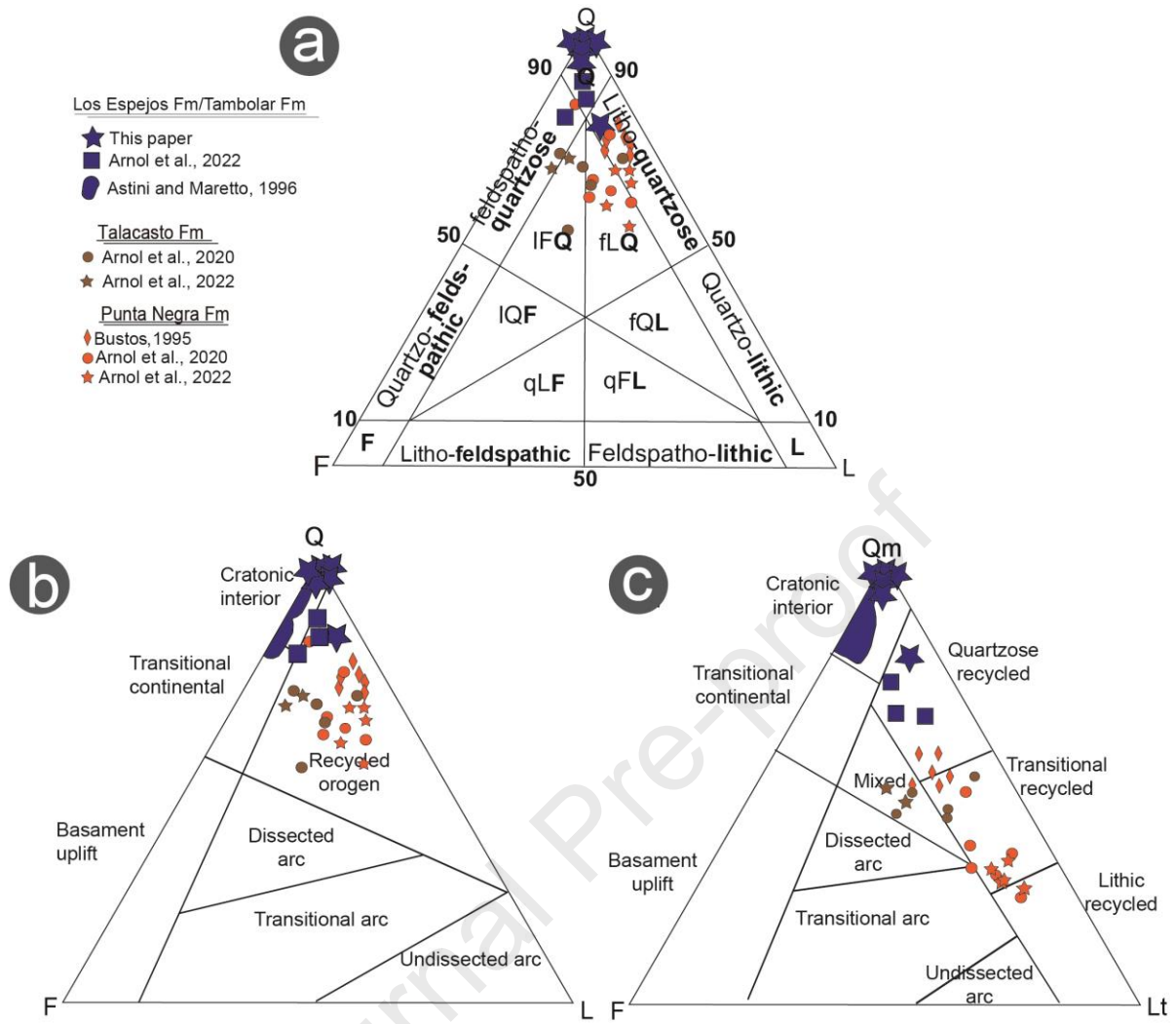


239

240 **Figure 2.** Microphotographs of the Los Espejos Formation samples. Scale bar: 200
 241 micrometers. Detail of the mantles where opaque and heavy minerals are concentrated. The
 242 rest of the elements are difficult to visualize because of the small grain size. Qm:
 243 monocrystalline quartz, Fk: K-feldspar, Bt: biotite, Gr: garnet, Zr: zircon, Op: opaque mineral.
 244 a, c) with parallel nicols. b, d) with crossed nicols.

245 According to the diagram of Garzanti (2016), the studied samples mainly fall in the quartzose
 246 field, except for one sample which falls in the Litho-quartzose field (Fig. 3a). The same
 247 samples mainly fall in the cratonic interior fields of the QFL (Fig. 3b) and QmFLt (Fig. 3c)
 248 diagrams of Dickinson et al. (1983), except for one sample which falls in the quartzose
 249 recycled field of the last diagram.

250

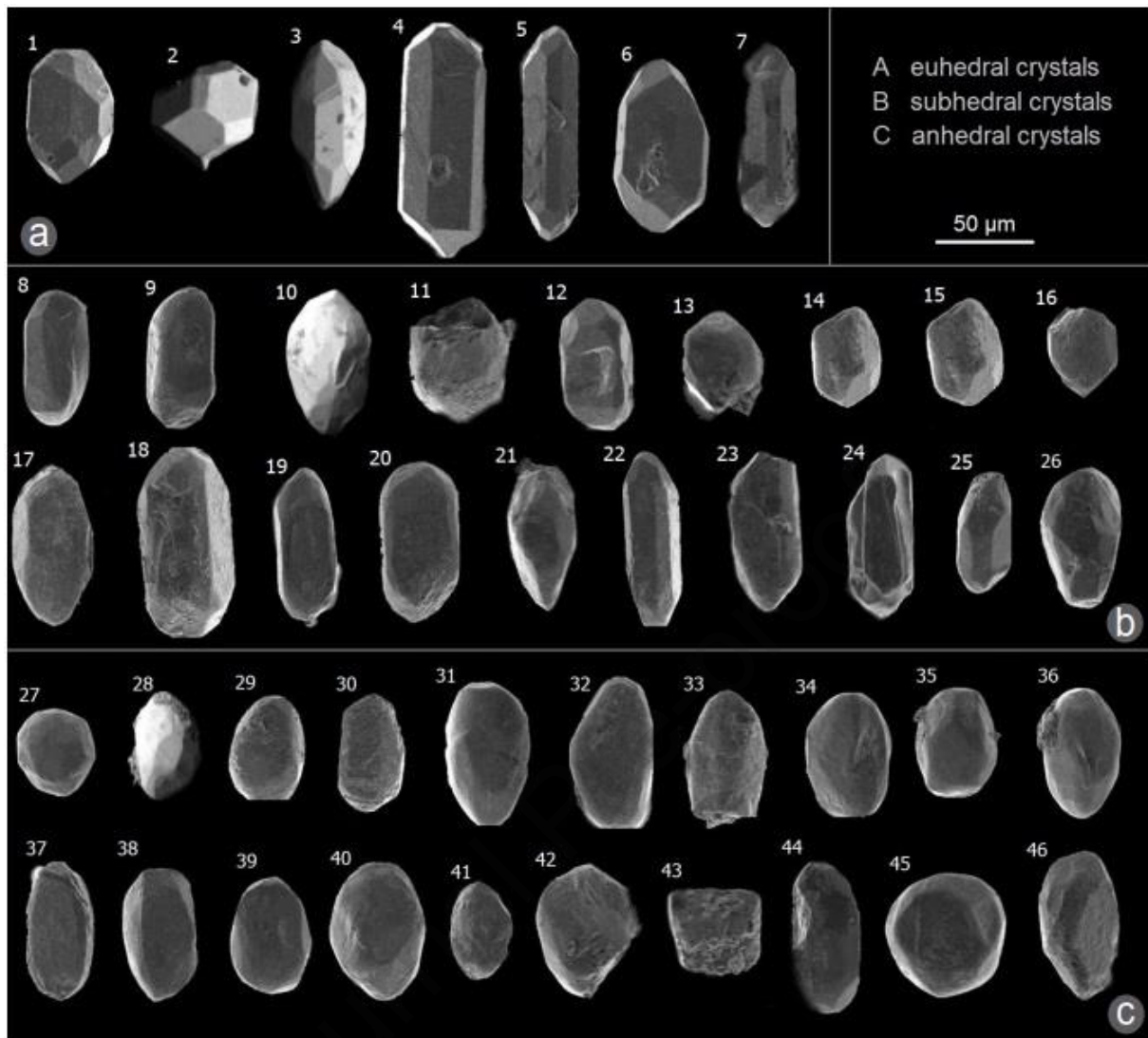


251

252 **Figure 3. a)** Ternary diagrams of lithological classification according to Garzanti (2016). **b, c)**
 253 Provenance diagrams of Dickinson et al. (1983). Q: quartzose, F: Feldspathic; L: lithic; IFQ:
 254 litho-feldspatho-quartzose; IQF: litho-quartzo-feldspathic; fLQ: feldspatho-litho-quartzose;
 255 fQL: feldspatho-quartzo-lithic; qFL: quartzo-feldspatho-lithic; qLF: quartzo-litho-feldspathic.

256 4.2 Morphological analysis of zircons

257 Forty-six photographs of detrital zircons were analyzed, of which 7 are euhedral grains, 19
 258 subhedral and 20 anhedral (Fig. 4).



259

260 **Figure 4.** Detrital zircons from sample 16LE29 (Los Espejos Formation) labeled from 1 to 46.

261 See text for information.

262

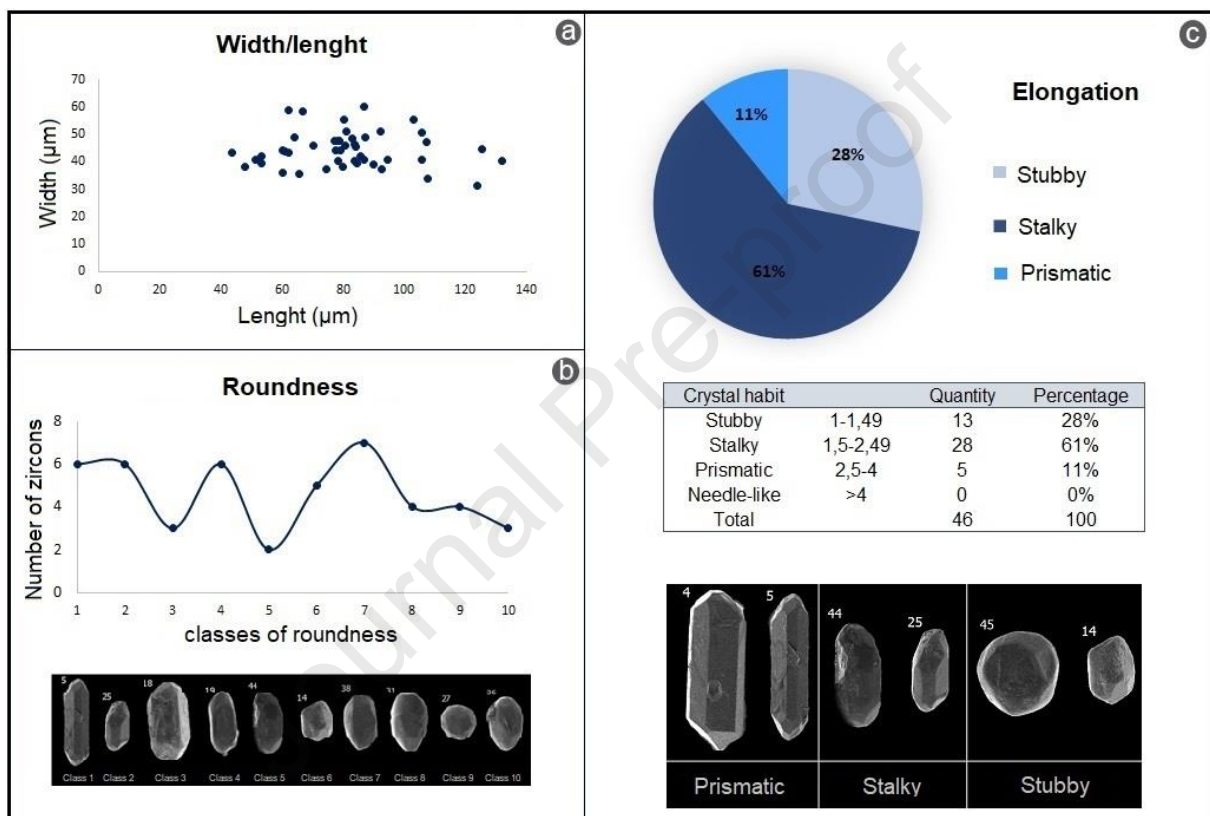
263 The size of the crystals is between 43.4 μm (n.43) and 131.9 μm (n.22) long, and between
 264 37.0 μm (n.25) and 60.4 μm (n.40) wide (Fig. 4b, c).

265 The relationship between the length and width of the crystals is shown in Figure 5a, being
 266 crystal n.5 (Fig. 4a) the one with the greatest elongation, with 3.94 and corresponding to the
 267 long-prismatic class, and crystal n.43 (Fig. 4c) the one with lowest elongation, with 1.10 and
 268 corresponding to the short-stubby class.

269 The degree of crystals roundness is variable, ranging from completely unrounded to
 270 completely rounded (classes 1 to 10 in the classification of Schneiderhöhn, 1954), with

271 classes 1, 2, 4 and 7 predominating over the rest (Fig. 5b). In this way, three main groups
 272 are recognized in the studied sample, suggesting different sources of contribution or degrees
 273 of transport.

274 Following the classification proposed by Mitterer (2001), three groups of zircons were defined
 275 according to their habit: stubby, stalky and prismatic. Taking into account their elongation,
 276 61% are stalky, 28% stubby and 11% prismatic (Fig. 5c).



277
 278 **Figure 5.** a) Length/width ratio of crystals. b) Number of zircons for each rounding class
 279 (Schneiderhöhn, 1954) with examples from the studied sample. c) Percentage of crystals for
 280 each elongation class (Mitterer, 2001) with examples from the studied sample.

281
 282 The predominant surface features are collision marks and fractures. The crystals were
 283 classified following the work and classifications proposed by Gärtner et al. (2013 and
 284 references therein). In this way, it was recognized that these features are present in 45% of
 285 zircons, belonging the euhedral crystals to classes 1 and 2, and the subhedral and anhedral
 286 crystals to the four classes. In addition, 15% of zircons have fractures, with 4% and 11% of

287 fractures parallel and perpendicular, respectively, to the *c* axis. Finally, only 3 zircons have
288 visible cracks (n.20, 23 and 31; Fig. 4b, c).

289 Of the total zircon crystals analyzed, only 32% could be classified according Pupin (1980)
290 because they preserved their crystalline faces. The crystals show a predominance of group
291 P, accompanied by some crystals with morphotypes S, R, and D that could be associated
292 with two feldspars granites.

293

294 *4.3 U-Pb analysis in detrital zircons*

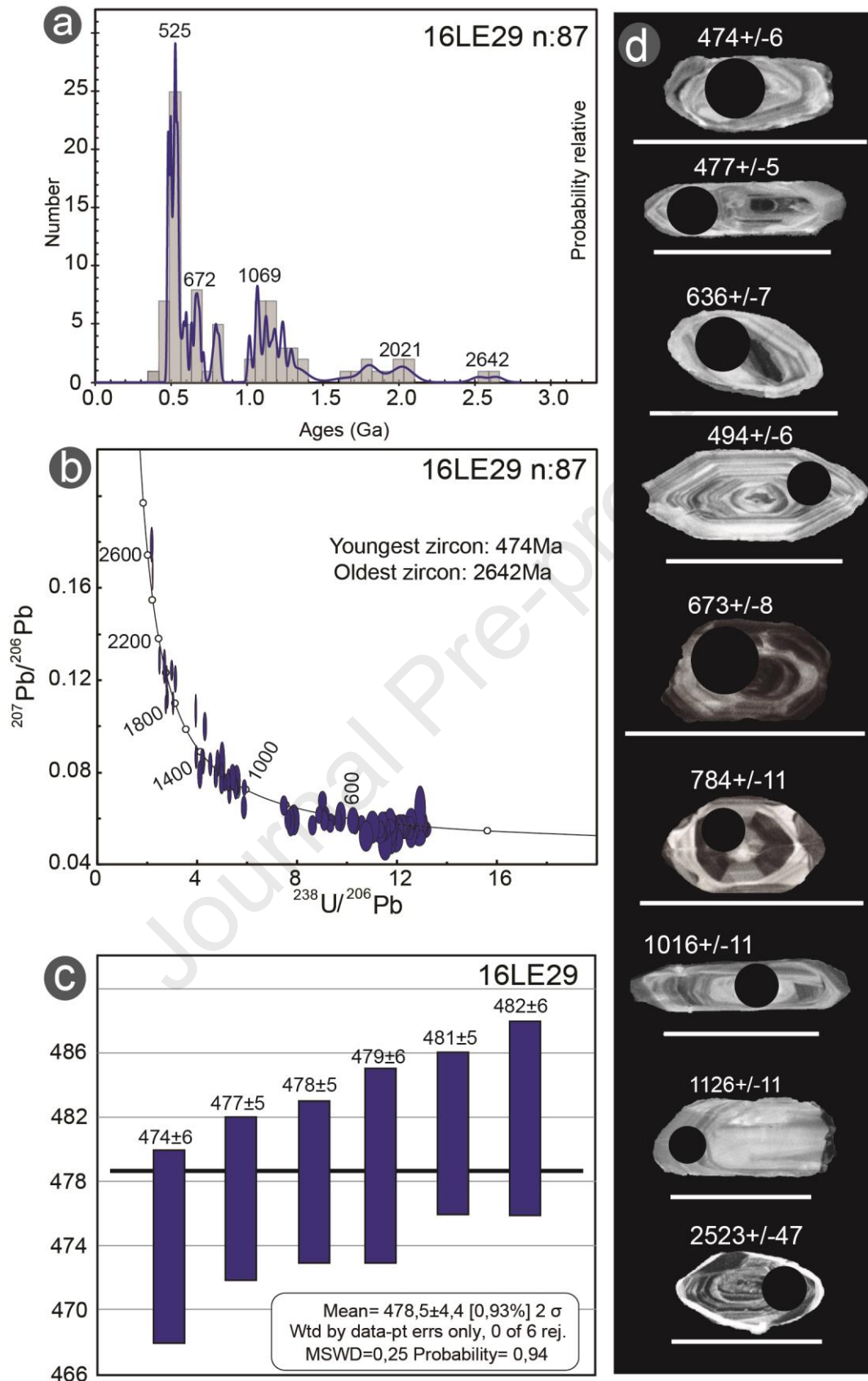
295 To achieve a better understanding of the distribution of the recorded ages, they were
296 grouped according to recognized orogenic cycles. The analysis of 87 detrital zircon grains
297 reveals a polymodal trend (Fig. 6a). The main mode is represented by ages belonging to the
298 Pampean-Brasiliano orogenic cycle (42.5%), of which 26.4% ages correspond to the
299 Neoproterozoic and 16.1% to the early Cambrian. The Grenvillian orogenic cycle is
300 represented by 28.7% grains with ages between 1354 and 1014 Ma (Ectasian-Stenian). The
301 Famatinian orogenic cycle is represented by 16.1% grains with ages between 507 and 474
302 Ma (late Cambrian-Devonian). Famatinian ages are distributed as follows: 3.6% in the middle
303 Cambrian, 5.7% in the late Cambrian and 6.8% in the Ordovician. Although a Devonian age
304 (400 Ma) was recorded, this value was not considered in the percentage calculation due to
305 its high common Pb (> 34%) and lack of concordance. The Paleoproterozoic and Archean
306 are represented by 10.3% (2078 - 1624 Ma) and 2.4% (2642 - 2523 Ma) grains, respectively,
307 and constitute the oldest ages (Fig. 6a, b).

308 From the peaks of ages generated by the youngest zircons, the maximum sedimentation age
309 of this sample was calculated, giving a value of 478.5 ± 4.4 Ma (Tremadocian; Fig. 6c). This
310 age is not consistent with the fossil record of the unit, corresponding to the Afro-South
311 American fauna, mainly assigned to the upper Silurian, but would be indicating an important
312 contribution from Ordovician sources at the time of deposition of the unit in the study region.
313 Figure 6d shows the cathodoluminescence images of the analyzed zircons, where it can be

314 seen that most of them present a concentric internal zonation, which allows them to be
315 interpreted as plutonic zircons.

316 These U-Pb data have been subjected to the Kolmogorov-Smirnoff statistical analysis (K-S
317 test), providing objective information of the degree of correlation between the different detrital
318 zircon populations of the compared samples (Table 2).

Journal Pre-proof



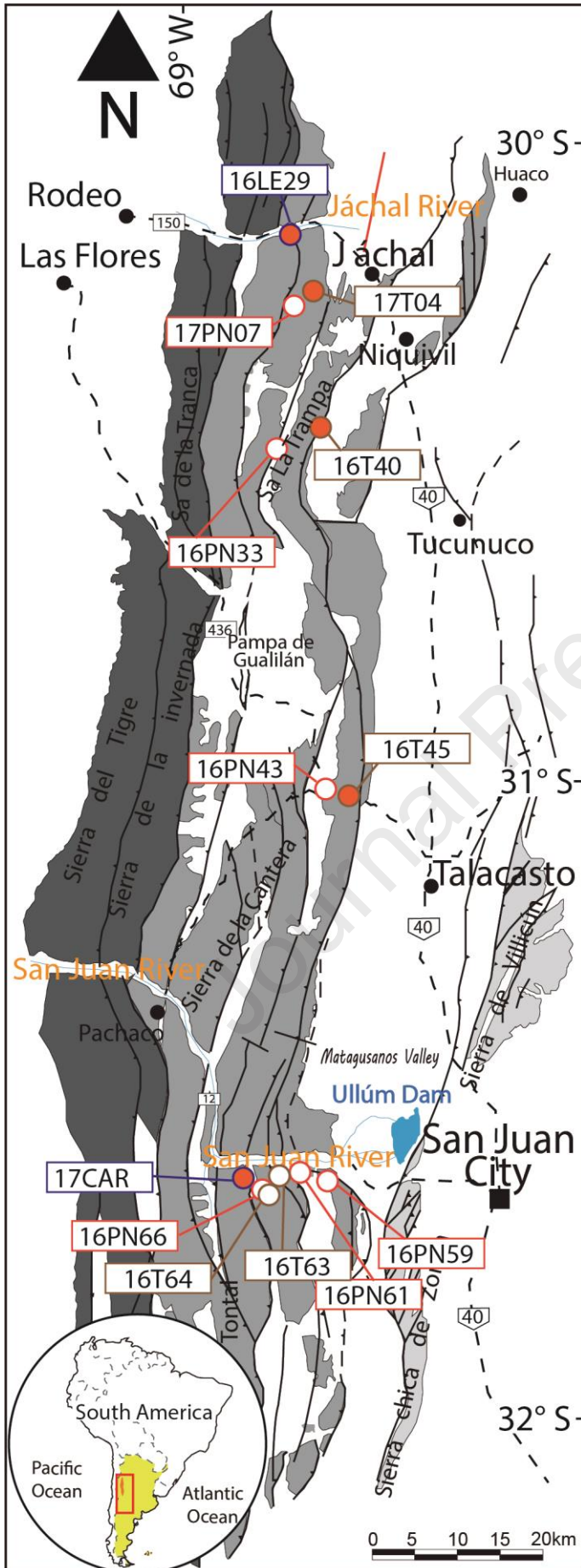
319

320 **Figure 6. a)** Relative probability diagram with U-Pb ages in detrital zircons for sample
 321 16LE29 from the Los Espejos Formation. **b)** Tera-Wasserburg diagram. a and b were

322 generated with the programme Isoplot/Ex (Ludwig, 2008). **c)** Maximum sedimentation age
323 (MSA) of sample 16LE29. **d)** Selected cathodoluminescence (CL) images, scale: 100 μm .

324

325 The Kolmogorov-Smirnov statistical test was performed comparing the Los Espejos
326 Formation with one sample of the Tambolar Formation (Arnol et al., 2022). In addition,
327 Silurian samples were compared with eleven samples of the Devonian Gualilán Group (Fig.
328 7; Arnol et al., 2020, 2022). From the K-S test (Table 2), a good correlation is observed
329 between Silurian samples, despite the fact they belong to very distant sectors / areas. In
330 Table 2 it is important to note that sample 16LE29 record a high correlation grade with
331 samples of the Talacasto Formation, mainly with those of the Northern region and whit some
332 samples of the Central region (Fig. 7). On the other hand, the Punta Negra Formation does
333 not show any correlation (Fig. 7 and Table 2).



335 **Figure 7.** Distribution of the samples analyzed by the U-P method and compared by the K-S
 336 test in this work and those analyzed by Arnol et al. (2020, 2022). The filled circles represent
 337 the samples with positive values of correlation with the Los Espejos Formation, while the
 338 empty ones respond to samples that are not possible to correlate with the Los Espejos
 339 Formation.

340
 341 In this way, it is possible to establish that the Los Espejos Formation share a common source
 342 with the Tambolar Formation and from the Talacasto Formation of the Northern region, near
 343 the town of San José de Jáchal and Quebrada de Talacasto area.

Formation	Los Espejos	Tambolar	Talacasto					Punta Negra					
Samples	16LE29	17CAR	17T04	16T40	16T45	16T63	16T64	17PN07	16PN33	16PN43	16PN59	16PN61	16PN66
16LE29		0.215	0.459	0.941	0.727	0.001	0.019	0.007	0.014	0.000	0.000	0.000	0.000
17CAR	0.215		0.011	0.898	0.700	0.002	0.001	0.155	0.088	0.000	0.000	0.000	0.000
17T04	0.459	0.011		0.789	0.159	0.000	0.109	0.002	0.001	0.000	0.000	0.000	0.000
16T40	0.941	0.898	0.789		0.846	0.313	0.163	0.327	0.182	0.000	0.000	0.000	0.001
16T45	0.727	0.700	0.159	0.846		0.000	0.003	0.069	0.036	0.000	0.000	0.000	0.000
16T63	0.001	0.002	0.000	0.313	0.000		0.049	0.000	0.001	0.000	0.000	0.000	0.000
16T64	0.019	0.001	0.109	0.163	0.003	0.049		0.000	0.000	0.000	0.000	0.000	0.000
17PN07	0.007	0.155	0.002	0.327	0.069	0.000	0.000		0.027	0.000	0.000	0.002	0.003
16PN33	0.014	0.088	0.001	0.182	0.036	0.001	0.000	0.027		0.000	0.000	0.000	0.000
16PN43	0.000	0.000	0.000	0.000	0.000	0.000	0.000	0.000	0.000		0.788	0.488	0.000
16PN59	0.000	0.000	0.000	0.000	0.000	0.000	0.000	0.000	0.000	0.788		0.694	0.003
16PN61	0.000	0.000	0.000	0.000	0.000	0.000	0.000	0.002	0.000	0.488	0.694		0.015
16PN66	0.000	0.000	0.000	0.001	0.000	0.000	0.000	0.003	0.000	0.000	0.003	0.015	

344
 345 **Table 2.** Kolmogorov-Smirnov (K-S) test of the studied samples. P-values of samples with
 346 correlation grade greater than 0.05 are shown in orange.

347

348 4.4 Lu-Hf analysis in detrital zircons

349 The analysis of the Lu-Hf isotopic ratios of 23 detrital zircon grains reveals the petrogenetic
 350 characteristics of the magmas from which they derive. The distribution of the parameters
 351 $\epsilon\text{Hf}_{(t)}$ and T_{DM} according to the U-Pb ages are as follows:

352 *Archean:* a single zircon of 2520 Ma was analysed. This crystal records an $\epsilon\text{Hf}_{(t)}$ value of 1
 353 and a T_{DM} model age of 2900 Ma (Fig. 8).

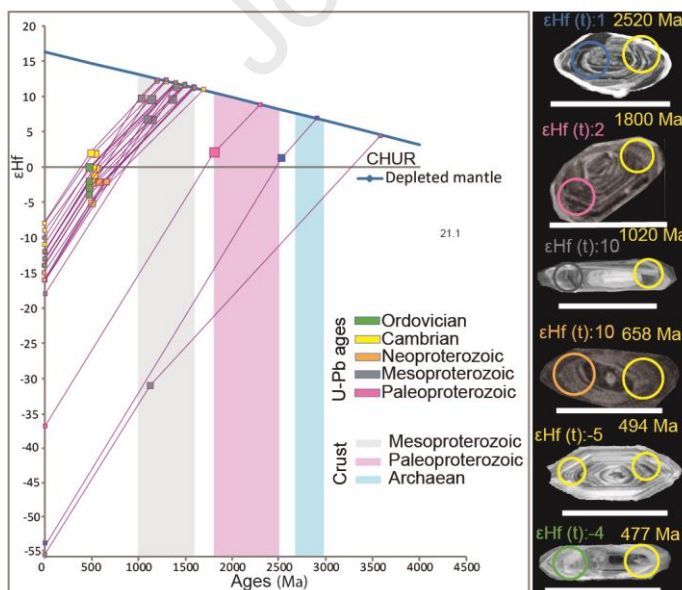
354 *Paleoproterozoic*: a single zircon of 1800 Ma was analyzed. This crystal records an $\epsilon\text{Hf}(t)$
 355 value of 2 and a T_{DM} model age of 2900 Ma (Fig. 8). As in the previous case, this T_{DM} model
 356 age indicates an origin related to an ancient Archean crust.

357 *Mesoproterozoic*: 7 zircon grains were analysed. A single Ectasian zircon (1350 Ma) gave
 358 $\epsilon\text{Hf}(t)$ and T_{DM} values of 2 and 2300 Ma, respectively. The remaining zircons are Stenian
 359 (1130 – 1080 Ma) and gave $\epsilon\text{Hf}(t)$ values of 7-10 as well as T_{DM} model ages of 1500-1200
 360 Ma, so they would have derived from a Mesoproterozoic crust. It should be noted that within
 361 this group it can be distinguished a zircon of 1130 Ma with an $\epsilon\text{Hf}(t)$ value of -31 and a T_{DM}
 362 model ages of 3600 Ma, indicating an origin related to an ancient Archean crust.

363 *Neoproterozoic*: for this interval, 3 grains were analyzed, obtaining $\epsilon\text{Hf}(t)$ and T_{DM} values of -2
 364 and 1600 Ma respectively (Fig. 8).

365 *Cambrian*: 8 zircon crystals exhibit $\epsilon\text{Hf}(t)$ values between -5 and 2, whereas the T_{DM} model
 366 ages range from 1700 to 1200 Ma so they would have derived from Mesoproterozoic and
 367 Paleoproterozoic crusts (Fig. 8).

368 *Ordovician*: 4 zircon crystals exhibit $\epsilon\text{Hf}(t)$ values between -4 and 0 whereas the T_{DM} model
 369 ages ranges from 1600-1400 Ma, so they would have derived from Mesoproterozoic crust
 370 (Fig. 8).



371
 372 **Figure 8.** ϵHf vs. ages diagram for detrital zircons of the Los Espejos Formation. The main
 373 T_{DM} model ages are mainly Mesoproterozoic and, in minor proportion, Paleoproterozoic and

374 Archaean. Examples of selected cathodoluminescence images showing the U-Pb (on the
375 right) and Lu-Hf (on the left) analysis points with their respective results.

376

377 **5. DISCUSSION**

378 The fact that the petrographically analysed samples of the Los Espejos Formation
379 correspond to quartzites does not necessarily indicate that the involved sediments derived
380 directly from a cratonic area, as indicated by Dickinson's et al. (1983) ternary diagrams. The
381 strong reworking of the sediments prior to lithification, also evidenced by zircon morphology,
382 resulted in a concentration of chemically mature clastic components with high percentages of
383 quartz and resistant heavy minerals such as zircon, rutile and tourmaline. Due to lithological
384 and faunal similarities, the Los Espejos Formation could be compared with the Tambolar
385 Formation (Heim, 1952) located near the San Juan River (Fig. 7). According to studies
386 carried out by Benedetto et al. (1992), Astini et al. (1995), and Astini and Maretto (1996),
387 both units would be equivalent and would have had common sedimentary sources. On the
388 other hand, due to the fact that the top unit of the Tucunuco Group (Los Espejos Formation)
389 is of early Lochkovian age towards its upper part in some sectors of the basin (Benedetto et
390 al., 1992), it could be comparable with the Talacasto Formation (basal unit of the Gualilán
391 Group). In this way, based on the comparison of ages of detrital zircon populations from the
392 Silurian and Devonian units, among other characteristics, an attempt was made to establish
393 whether there were no changes in the contribution of sediment sources during this
394 depositional interval. The Los Espejos Formation has predominance of stalky crystals and
395 collision marks, and has similar roundness patterns. The analyzed detrital zircons of the
396 Tambolar Formation present similar characteristic (Arnol et al., 2022). According to Pupin's
397 (1980) classification, both Silurian sequences (i.e., Los Espejos and Tambolar formations)
398 would have derived from subsolvus granites. The only observable difference is that the Los
399 Espejos Formation has larger zircons than the Tambolar Formation, although the zircons
400 respect the length-width ratios, so the elongation parameters are similar in both units
401 (Cretacotta, 2022). Regarding the Talacasto Formation (sample 16T45 in Arnol et al., 2020),

402 it presents crystals with well-developed crystalline faces, larger sizes, higher elongation
403 values, and fewer crystals with fractures, which indicate that the sources of detrital zircons
404 could have varied, but that the plutonic igneous origin was maintained.

405 For the Los Espejos Formation, relative to the Talacasto Formation, a smaller number of
406 zircons were analyzed using Pupin's (1980) classification because the proportion of zircons
407 with recycling characteristics increases in this Silurian unit. Nevertheless, in both cases,
408 morphotype P is predominant, referring to subsolvus granites. With this information, it could
409 be estimated that recycled zircons dominate in both units, being the rest associated with a
410 plutonic origin. However, compared with the Talacasto Formation, there is less development
411 of crystalline faces in zircons, which could be originated by reworking of sediments previous
412 to lithification/diagenesis. This could be due to the fact that the sediment rocks of the Los
413 Espejos Formation recorded more than one sedimentation cycle or that the contribution
414 areas of the sequence are farther away, which is why the transport of the crystals was
415 increased until their final deposition. This last hypothesis could be applied to the
416 Paleoproterozoic and Archean zircons, since there are no nearby rocks that record these
417 ages, with age records and Hf parameters coinciding with rocks from Río de la Plata Craton,
418 where it is possible to find heterogeneous $\epsilon\text{Hf}(t)$ values. Considering last parameter and the
419 T_{DM} model ages, we can suggest that the oldest zircons from the Los Espejos Formation
420 derived from Tandilia terrane of Argentina (Cingolani et al., 2010; Santos et al., 2017;
421 Angeletti et al., 2021) instead of the Piedra Alta terrane of Uruguay, where the $\epsilon\text{Hf}(t)$ values
422 turn out to be very positive or very negative in the different types of rocks analyzed (Oriolo et
423 al., 2016). For its turn, the first hypothesis is more difficult to verify because it is an old unit.
424 The uplift of the Grenvillian orogen, which have been postulated for the Devonian (Arnol et
425 al., 2020, 2022), could had started in Silurian times. This would leave as a result that the pre-
426 Silurian sedimentary units which have Neoproterozoic-Cambrian and Mesoproterozoic
427 records could have also acted as source areas, indicating that although the distances are
428 reduced from the source rock to the basin, they could have gone through more than one
429 sedimentation cycle.

430 The considerable contributions from Neoproterozoic sources in the northern region (study
431 area) for the compared samples allow us to infer that the sediment sources, were the same
432 during the Late Silurian and Devonian. The significant difference in the participation of
433 cratonic sources would indicate higher exhumation rates of cratonic areas for the Silurian,
434 which are found in a very reduced or non-existent manner in the upper unit of the Gualilán
435 Group. However, the differences in the populations of registered ages are very significant for
436 the southern region. This is reinforced by the null correlation values between the compared
437 areas, indicating that for this sector of the basin there is evidence of a change in the
438 sediment sources, at least for Paleoproterozoic ages that are present in the Silurian units
439 and are practically absent in the Devonian sequences. This could be linked to what is already
440 suggested by Arnol et al. (2022), who pointed out a greater exhumation of the
441 Mesoproterozoic (Grenvillian) orogen which would have acted as a continuous topographic
442 barrier preventing the entry of sediments located to the east of it.

443

444 *5.1 Potential rock sources*

445 The U-Pb data from the Los Espejos Formation samples are composed of a clear dominance
446 of Pampean-Brasiliano sources. Basement rocks of early Cambrian age (Fig. 9) are found in
447 the Eastern Pampean Ranges, as for example in Sierra Chica, Sierra Grande, Sierra de
448 Pocho, Sierra de Comechingones, Sierra Norte de Córdoba and Sierra Sur de Santiago del
449 Estero (Gordillo, 1996; Rapela et al., 1998; Sims et al., 1998; Gromet and Simpson, 1999;
450 Candiani et al., 2001; Escayola et al., 2007; Tibaldi et al., 2008; Iannizzotto et al., 2013;
451 Baldo et al., 2014; D'Eramo et al., 2014; Lira et al., 2014; Ramos et al., 2015; Dahlquist et
452 al., 2016; among others). Despite the numerous works that have provided U-Pb ages of
453 basement rocks from these mountains, works with Lu-Hf data are still scarce. The availability
454 of this isotopic pair would allow greater certainty about the characteristics of magmas from
455 which zircons derived, and would help to clearly identify the rocks that contributed to the
456 basin. The data provided by Dahlquist et al. (2016) for the Guasayán pluton yielded a U-Pb
457 crystallization age of 533 ± 4 Ma and $\epsilon_{\text{Hf}(t)}$ values between -4.76 and -0.12, indicating that

458 rocks with these characteristics could have been the precursor sources of the early
459 Cambrian zircons recorded in the Los Espejos Formation.

460 In the Eastern Cordillera, many authors provided U-Pb ages for granitoids of the Santa Rosa
461 de Tastil Batholith (Fig. 9) (Bachmann et al., 1987; Hongn et al., 2010; Escayola et al., 2011;
462 Hauser et al., 2011; Lucassen et al., 2011; Ortiz et al., 2017). On the other hand, Bachmann
463 et al. (1987) and Escayola et al. (2011), among others, analyzed granitoids of the Cañani
464 Batholith, obtaining early Cambrian ages between 537 and 519 Ma. These rocks are not
465 ruled out as sediment sources, because the $\epsilon_{\text{Hf}(t)}$ values provided by Hauser et al. (2011)
466 and Ortiz et al. (2017) coincide with the $\epsilon_{\text{Hf}(t)}$ values recorded in the Cambrian detrital zircons
467 of the Los Espejos Formation. For its part, in the Puna it is also possible to record these
468 ages, for example in Sierra de Los Cobres or Sierra de Calalaste (Hauser et al., 2008;
469 Zimmermann et al., 2014; among others), but unfortunately there are still no Lu-Hf data for
470 these rocks that allow us to confirm or rule out these rock as sources areas (Fig. 9).

471 On the other side, Neoproterozoic sources are constrained to the Western Pampean Ranges
472 (e.g., Sierra Pie de Palo), with ages ranging from 850 to 600 Ma and $\epsilon_{\text{Hf}(t)}$ values between -3
473 and 10 (Baldo et al., 2006; Martin et al., 2020), which coincide with data obtained in this
474 work. Other possible sources for zircons with these ages are found in Sierra de Umango and
475 Sierra de Maz, where granitoids, paragneiss, schists and meta-sedimentary rocks with U-Pb
476 ages between 850 and 700 Ma crop out (Varela et al., 2011; Rapela et al., 2016).

477 The Mesoproterozoic sources are widespread in the Western Pampean Ranges: in Sierra de
478 Umango (Fig. 9), Varela et al. (2011) provided a TIMS U-Pb zircon upper intercept age
479 (crystallization age) of 1108 ± 4 Ma in an amphibolite of the Tambillito Formation. For the
480 Maz Complex, cropping out in the homonymous range, different authors provided ages
481 between 1330 and 1086 Ma (Casquet et al., 2006; Rapela et al., 2010, among others). On
482 the other hand, in Sierra de Pie de Palo, McDonough et al. (1993), Casquet et al. (2001),
483 Vujovich et al. (2004), Morata et al. (2008) and Rapela et al. (2010), among others, provided
484 different ages obtained for rocks of the Pie de Palo Complex, with values between 1200 and
485 1000 Ma. However, these ages are not exclusive from this geological province, but it is

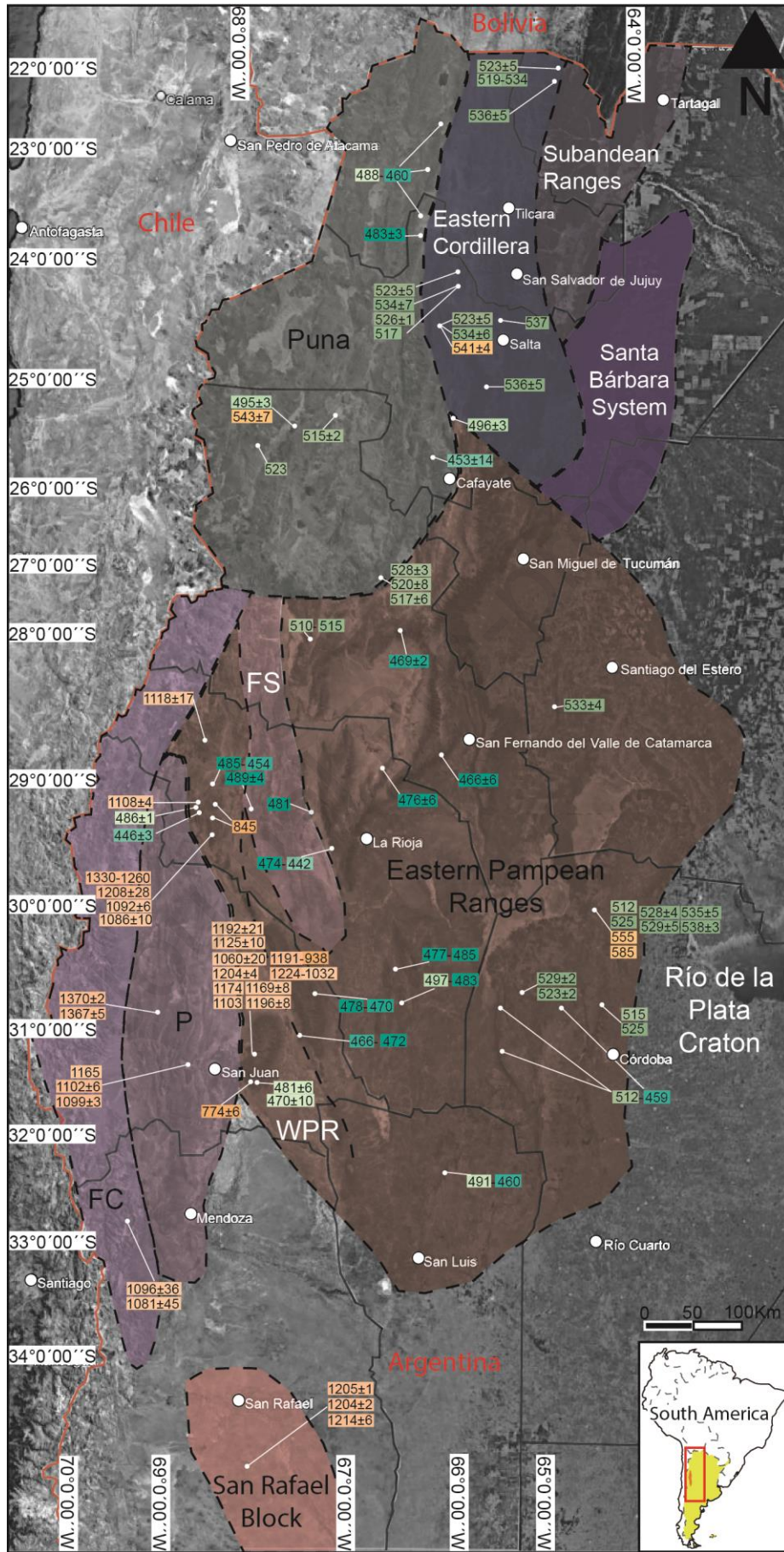
486 possible to find them in the Precordillera. To the north of the Precordillera, the Río Bonete
487 Complex is recognized, there a mylonitic granite included in the Jagué shear belt, yielded a
488 U-Pb age of 1118 ± 17 Ma (Martina et al., 2005). Additionally, in basement xenoliths found in
489 the San Juan River area, Abbruzzi et al. (1993), Kay et al. (1996) and Martin et al. (2020),
490 among others, indicated Grenvillian U-Pb crystallization ages between 1188 to 1096 Ma for
491 the analyzed rocks (e.g., mafic xenolith, acid xenolith para-gneiss xenolith), as well as a U-
492 Pb metamorphic age of 1060 Ma for the same zircons (Rapela et al., 2010). Also in the
493 Precordillera, but as granitic clasts immersed in the matrix of the Los Sombreros Formation,
494 Thomas et al. (2012) recorded U-Pb crystallization ages close to 1370 Ma. Extending further
495 south in the San Rafael Block, Thomas et al. (2012) Cingolani et al. (2017) obtained U-Pb
496 crystallization ages around 1204 Ma for the Ponón Trehue Granite.

497 The Lu-Hf data obtained by Martin et al., (2020) for Mesoproterozoic zircons from different
498 locations within the Western Pampean Ranges and the San Rafael Block indicate that their
499 rocks would be the sediment sources. Mesoproterozoic zircons show juvenile characters,
500 with positive $\epsilon\text{Hf}_{(t)}$ values and mostly Mesoproterozoic T_{DM} model ages. For practically all the
501 Mesoproterozoic zircons of the Los Espejos Formation, the recorded positive values are
502 identical to those found in the Western Pampean Ranges and San Rafael Block.

503 The Ordovician granitoids are restricted to outcrops of the Famatinian Arc. Rocks related to
504 this magmatic event are mainly found in the Famatina System. However, it is possible to find
505 identical ages, to a lesser degree of representativeness, in other geological provinces such
506 as the Eastern Pampean Ranges or the Puna. Several authors presented U-Pb ages
507 between 493 and 442 Ma for rock related to the Famatinian orogenic cycle (Dahlquist, 1999;
508 Dahlquist et al., 2008, 2013; Pankhurst and Rapela, 1998; Pankhurst et al., 1998, 2000,
509 2008; Baldo et al., 2001, 2005; Varela et al., 2008, 2011; Casquet et al., 2012; Bellos et al.,
510 2015, 2020; among others). Dahlquist et al. (2013) provided $\epsilon\text{Hf}_{(t)}$ values between -14.7 and
511 3.3 for different granitoids of the Eastern Pampean Ranges and the Famatina System.
512 Recently, Martin et al. (2020) reported $\epsilon\text{Hf}_{(t)}$ values between -5 and 0 for Famatinian
513 granitoids from La Rioja Province. These results are identical to those found in Ordovician

514 ages detrital zircons present in the Los Espejos Formation, so it can be deduced that the
515 Famatinian granitoids were the source area for these zircons.

Journal Pre-proof



517 **Figure 9.** Time–space plot of Proterozoic and early Paleozoic (Cambrian-Ordovician)
518 plutonic and metamorphic rocks on the western Gondwana margin at 22°–35°S, displaying
519 the main regions discussed in the text as possible sediment sources. The figure shows
520 plutonic and metamorphic outcrops, including U–Pb zircon data. The colors of the boxes are
521 consistent with the color scale adopted by the IUGS. The works considered for this figure are
522 cited in Section 5.1. Abbreviations: FS: Famatina System P: Precordillera, FC: Frontal
523 Cordillera, WPR: Western Pampean Ranges.

524

525 FINAL REMARKS

- 526 • The petrographic analysis of the Los Espejos Formation shows that this unit is mostly
527 composed of quartz-bearing rocks classified as quartzites. The unit also contains iron
528 rich mantles. The morphology of detrital zircons indicates mainly recycled sources.
529 Recycled zircons from relatively nearby source rocks could be linked to more than
530 one sedimentation cycle. In addition to this evidence, the low participation of ancient
531 sources leads us to conclude that, for this case, the diagrams of Dickinson et al.
532 (1983) do not reflect to the sedimentary history of the rock analyzed, since they would
533 not derive from a cratonic area, but from a recycled orogen that suffered repeated
534 sedimentation cycles.
- 535 • The Los Espejos Formation has a clear predominance of Neoproterozoic to early
536 Cambrian sources. As a secondary mode, there are Mesoproterozoic sources,
537 mainly Stenian. In similar percentages, the Famatinian sources are recorded with
538 scarce contribution of ancient sources.
- 539 • The maximum sedimentation age for sample 16LE29 corresponds to the
540 Tremadocian (478.5 ± 4.4 Ma), indicating that the youngest sources that contributed
541 sediments to this region of the basin correspond to rocks of the Famatinian Orogen.

- 542 • The Lu-Hf data indicate that the main areas of sediment contribution were the
543 Western Pampean Ranges and the Famatina System, whose zircons derived mainly
544 from a Mesoproterozoic crust.
- 545 • The Los Espejos Formation shares sediment sources with the Tambolar Formation, in
546 the San Juan River area and with the Talacasto Formation in the north of the basin.
547 The difference between the Silurian samples and the Talacasto Formation in the San
548 Juan River area would be linked to paleogeographic changes within the basin and
549 along its edges, which influenced the amounts of zircons grains of different ages that
550 arrived and were recorded for the different areas.

551

552 **Acknowledgements**

553 This research was partially financed by the Consejo Nacional de Investigaciones Científicas
554 y Técnicas (CONICET) of Argentina and the Universidad Nacional de La Plata (UNLP)
555 through the research grants PUE-CIG and PIPD/N040, respectively. The authors would like
556 to acknowledge the División Geología (Museo de La Plata-UNLP), the Centro de
557 Investigaciones Geológicas (CIG, CONICET-UNLP) and the Centro de Pesquisas
558 Geocronológicas (CPGeo, Universidade de São Paulo) for provided their facilities for sample
559 preparations and isotopic analysis. We warmly acknowledge the comments and suggestions
560 of an anonymous reviewer and of the Editor-in-Chief Andrés Folguera, which considerably
561 improved the original manuscript.

562

563 **REFERENCES**

564 Abre, P., Cingolani, C.A., Cairncross, B., Chemale, F., 2012. Siliciclastic Ordovician
565 to Silurian units of the Argentine Precordillera: Constraints on provenance and tectonic
566 setting in the proto-Andean margin of Gondwana. *Journal of South American Earth Sciences*,
567 40, 1-22.

568 Abbruzzi, J.M., Kay, S.M., Bickford, M.E., 1993. Implications for the nature of the
569 Precordilleran basement from the geochemistry and age of Precambrian xenoliths in
570 Miocene volcanic rocks, San Juan province. XII Congreso Geológico Argentino y II Congreso
571 de Exploración de Hidrocarburos, Mendoza, Actas, 3, 331-339.

572 Angeletti, M., Chichorro, M., Castro, A., Frisicale, M.C., Solá, R., Dimieri, L.V., 2021.
573 New geochemical, U–Pb SIMS geochronology and Lu–Hf isotopic data in zircon from
574 Tandilia basement rocks, Río de la Plata craton, Argentina: evidence of a sanukitoid
575 precursor for some Paleoproterozoic granitoids. *Journal of South American Earth Sciences*,
576 108, 103199.

577 Arnol, J.A., Uriz, N.J., Cingolani, C.A., Basei, M.A.S., Abre, P., 2020. Provenance
578 analysis of Devonian peripheral foreland basins in SW Gondwana, case of the Gualilán
579 Group, Precordillera Argentina. *International Journal of Earth Sciences*, 109, 2467-2494.

580 Arnol, J.A., Uriz, N.J., Cingolani, C.A., Abre, P., Basei, M.A.S., 2022. Provenance
581 evolution of the San Juan Precordillera Silurian-Devonian basin (Argentina): Linking with
582 other depocentres in Cuyania terrane. *Journal of South American Earth Sciences*, 115,
583 103766.

584 Astini, R.A., 1992. Tectofacies ordovícicas y evolución de la cuenca eopaleozoica de
585 la Precordillera Argentina. *Estudios Geológicos*, 48, 315-327.

586 Astini, R.A., Benedetto, J.L., Vaccari, N.E., 1995. The early Paleozoic evolution of the
587 Argentine Precordillera as a Laurentian rifted, drifted, and collided terrane: A geodynamic
588 model. *Geological Society of America Bulletin*, 107, 253-273.

589 Astini, R.A., Maretto, H.M., 1996. Análisis estratigráfico del Silúrico de la Precordillera
590 Central de San Juan y consideraciones sobre la evolución de la cuenca. XIII Congreso
591 Geológico Argentino and III Congreso de Exploración e Hidrocarburos, Buenos Aires, Actas
592 1, 351-368.

593 Bachmann, G., Grauert, B., Kramm, U., Lork, P., Miller, H., 1987. El magmatismo del
594 Cámbrico medio-Cámbrico superior en el basamento del Nordeste argentino:

595 investigaciones isotópicas y geocronológicas sobre los granitoides de los complejos
596 intrusivos de Santa Rosa de Tastil y Cañani. X Congreso Geológico Argentino. 125-127.

597 Baldis, B.A.J., 1970. Estratigrafía del Devónico de la Precordillera entre los paralelos
598 30° y 32°. Universidad de Buenos Aires, Unpublished PhD thesis, 168.

599 Baldis, B.A.J., Bordonaro, O., Beresi, M., Uliarte, E., 1981. Zona de dispersión
600 estromatolítica en la secuencia calcareo-dolomítica del Paleozoico Inferior de San Juan. IIX
601 Congreso Geológico Argentino, Buenos Aires. Actas 1, 419-434.

602 Baldo, E., Casquet, C., Rapela, C.W., Pankhurst, R.J., Galindo, C., Fanning, C.M.,
603 Saavedra, J., 2001. Ordovician metamorphism at the southwestern margin of Gondwana: PT
604 conditions and U-Pb SHRIMP ages from Loma de las Chacras, Sierras Pampeanas. III
605 South American Symposium on Isotope Geology, 3, 544-547.

606 Baldo, E., Dahlquist, J., Rapela, C.W., Casquet, C., Pankhurst, R. J., Galindo, C.,
607 Fanning, C.M., 2005. Early Ordovician peraluminous magmatism in the Sierra de Pie de Palo
608 (Western Sierras Pampeanas): geotectonic implications. International Congress Gondwana
609 12, Abstracts Academia Nacional de Ciencias. Argentina, 57.

610 Baldo, E., Casquet, C., Pankhurst, R.J., Galindo, C., Rapela, C.W., Fanning, C.M.,
611 Murra, J., 2006. Neoproterozoic A-type magmatism in the Western Sierras Pampeanas
612 (Argentina): evidence for Rodinia break-up along a proto-lapetus rift. *Terra Nova*, 18, 388-
613 394.

614 Baldo, E.G., Rapela, C.W., Pankhurst, R.J., Galindo, C., Casquet, C., Verdecchia, S.
615 O., Murra, J., 2014. Geocronología de las Sierras de Córdoba: revisión y comentarios.
616 *Geología y Recursos Naturales de la Provincia de Córdoba*, Asociación Geológica
617 Argentina, Córdoba, 845-868.

618 Benedetto, J.L., Racheboeuf, P.R., Herrera, Z., Brussa, E.D., Toro, B.A., 1992.
619 *Brachiopodes et biostratigraphie de la formation de Los Espejos, Siluro-Devonien de la*
620 *Precordillere (NW Argentine)*. *Geobios*, 25, 599-637.

- 621 Benedetto, J.L., Peralta, P., Sánchez, T.M., 1996. Morfología y biometría de las
622 especies de *Clarkeia kozlowski* (Brachiopoda, Rhynchonellida) en el Silúrico de la
623 Precordillera argentina. *Ameghiniana*, 33, 279-299.
- 624 Braccacini, O.I., 1949. El perfil de Tambolar. *Revista de la Asociación Geológica*
625 *Argentina* 4, 165-179.
- 626 Bellos, L.I., Castro, A., Díaz-Alvarado, J., Toselli, A., 2015. Multi-pulse cotectic
627 evolution and in-situ fractionation of calc-alkaline tonalite–granodiorite rocks, Sierra de
628 Velasco batholith, Famatinian belt, Argentina. *Gondwana Research*, 27, 258-280.
- 629 Bellos, L.I., Díaz-Alvarado, J., López, J.P., Rodríguez, N., Nagle, A.E.A., Tassinari,
630 C.C.G., Schleicher, A., 2020. The juxtaposition of Cambrian and early Ordovician
631 magmatism in the Tafí del Valle area. Characteristics and recognition of Pampean and
632 Famatinian magmatic suites in the easternmost Sierras Pampeanas. *Journal of South*
633 *American Earth Sciences*, 104, 102878.
- 634 Bustos, U.D., 1995. Sedimentología y evolución paleoambiental de la Formación
635 Punta Negra en el sector central de la Precordillera de San Juan. Trabajo Final, Facultad de
636 Ciencias Exactas, Físicas y Naturales, Universidad Nacional de Córdoba, Unpublished, 120
637 pp.
- 638 Candiani, J.C., Carignano, C., Stuart-Smith, P., Lyons, P., Miró, R., López, H.,
639 Skirrow, R., 2001. Hoja Geológica 3166-II Cruz del Eje, Provincias de Córdoba, La Rioja y
640 Catamarca. Boletín, unpublished. Servicio Geológico Minero Argentino.249.
- 641 Casquet, C., Baldo, E., Pankhurst, R.J., Rapela, C.W., Galindo, C., Fanning, C.M.,
642 Saavedra, J., 2001. Involvement of the Argentine Precordillera Terrane in the Famatinian
643 mobile belt: geochronological (U–Pb SHRIMP) and metamorphic evidence from the Sierra de
644 Pie de Palo. *Geology*, 29, 703–706.
- 645 Casquet, C., Pankhurst, R.J., Fanning, C.M., Baldo, E., Galindo, C., Rapela, C.W.,
646 Dahlquist, J.A., 2006. U–Pb SHRIMP zircon dating of Grenvillian metamorphism in Western
647 Sierras Pampeanas (Argentina): Correlation with the Arequipa-Antofalla craton and
648 constraints on the extent of the Precordillera Terrane. *Gondwana Research*, 9, 524-529.

649 Casquet, C., Rapela, C.W., Pankhurst, R.J., Baldo, E., Galindo, C., Fanning, C.M.,
650 Dahlquist, J., 2012. Fast sediment underplating and essentially coeval juvenile magmatism in
651 the Ordovician margin of Gondwana, Western Sierras Pampeanas, Argentina. *Gondwana*
652 *Research*, 22, 664-673.

653 Cingolani, C.A., Santos, J.O.S., Griffin, W., 2010. New insights of the
654 Paleoproterozoic basement of Tandilia belt, Río de la Plata Craton, Argentina: first Hf isotope
655 studies on zircon crystals. Symposium GEOSUR, Extended Abstract, Mar del Plata,
656 Argentina, 21-24.

657 Cingolani, C.A., Manassero, M., Basei, M., Uriz, N., 2013. Provenance of the
658 Villavicencio Formation (Lower Devonian) in the southern sector of the Precordillera,
659 Mendoza, Argentina: new sedimentary and geochronological data. I Congreso de Minería y
660 Geología del Cono Sur. Montevideo. Actas 1, 191-196.

661 Cingolani, C.A., Basei, M.A.S., Varela, R., Llambías, E.J., Chemale Jr., F., Abre, P.,
662 Uriz, N.J. Marque, J., 2017. The Mesoproterozoic basement at the San Rafael Block,
663 Mendoza Province (Argentina): Geochemical and Isotopic Age constraints. In: Cingolani,
664 C.A. (ed.). *Pre-Carboniferous Evolution of the San Rafael Block, Argentina*. Springer Earth
665 System Sciences, 19-58.

666 Cretacotta, A., 2022. Análisis petrográfico y de minerales pesados de la Formación
667 Los Espejos/Tambolar, Silúrico de la Precordillera Central sanjuanina: interpretación
668 preliminar de la procedencia sedimentaria. Trabajo final de licenciatura, Universidad
669 Nacional de La Plata, unpublished, 84 pp.

670 Cuerda, A.J., 1965. *Monograptus leintwardinensis* var. *incipiens* Wood en el Silúrico
671 de la Precordillera. *Ameghiniana*, 4, 171-177.

672 Cuerda, A.J., 1969. Sobre las graptofaunas del Silúrico de San Juan, Argentina.
673 *Ameghiniana*, 6, 223-235.

674 Cuerda, A.J., Rickards, R.B., Cingolani, C., 1988. A new Ordovician–Silurian
675 boundary section in San Juan Province, Argentina, and its definitive graptolite fauna. *Journal*
676 *of the Geological Society*, 145, 749-757.

677 Dahlquist, J.A., 1999. Significado petrogenético del epidoto en las granodioritas
678 famatinianas de la Sierra de Chepes, Argentina. Boletín de la Sociedad Española de
679 Mineralogía, 22, 33-34.

680 Dahlquist, J.A., Pankhurst, R.J., Rapela, C.W., Galindo, C., Alasino, P.H., Fanning, C.
681 M., Baldo, E.G., 2008. New SHRIMP U-Pb data from the Famatina Complex. Geológica
682 Acta, 319-333.

683 Dahlquist, J.A., Pankhurst, R.J., Gaschnig, R.M., Rapela, C.W., Casquet, C., Alasino,
684 P.H., Baldo, E.G., 2013. Hf and Nd isotopes in Early Ordovician to Early Carboniferous
685 granites as monitors of crustal growth in the Proto-Andean margin of Gondwana. Gondwana
686 Research, 23, 1617-1630.

687 Dahlquist, J.A., Verdecchia, S.O., Baldo, E.G., Basei, M.A., Alasino, P.H., Urán, G.A.,
688 Zandomeni, P.S., 2016. Early Cambrian U-Pb zircon age and Hf-isotope data from the
689 Guasayán pluton, Sierras Pampeanas, Argentina: implications for the northwestern boundary
690 of the Pampean arc. Andean Geology, 43, 137-150.

691 D'Eramo, F.J., Pinotti, L.P., Bonalumi, A., Sfragulla, J., Demartis, M., Coniglio, J.,
692 Baldo, E.G., 2014. El magmatismo ordovícico en las Sierras Pampeanas de Córdoba. En
693 Geología y recursos naturales de la provincia de Córdoba II. XIX Congreso Geológico
694 Argentino, 233-254.

695 Dickinson, W.R., Beard, L.S., Brackenridge, G.R., Erjavec, J.L., Ferguson, R.C.,
696 Inman, K.F., Ryberg, P.T., 1983. Provenance of North American Phanerozoic sandstones in
697 relation to tectonic setting. Geological Society of America Bulletin, 94, 222-235.

698 Dickinson, W.R., Gehrels, G.E., 2003. U-Pb ages of detrital zircons from Permian
699 and Jurassic eolian sandstones of the Colorado Plateau, USA: paleogeographic implications.
700 Sedimentary Geology, 163, 29-66.

701 Escayola, M.P., Pimentel, M.M., Armstrong, R., 2007. Neoproterozoic backarc basin:
702 Sensitive high-resolution ion microprobe U-Pb and Sm-Nd isotopic evidence from the
703 Eastern Pampean Ranges, Argentina. Geology, 35, 495-498.

704 Escayola, M.P., van Staal, C.R., Davis, W.J., 2011. The age and tectonic setting of
705 the Puncoviscana Formation in northwestern Argentina: An accretionary complex related to
706 Early Cambrian closure of the Puncoviscana Ocean and accretion of the Arequipa-Antofalla
707 block. *Journal of South American Earth Sciences*, 32, 438-459.

708 Gärtner, A., Linnemann, U., Sagawe, A., Hofmann, M., Ullrich, B., Kleber, A., 2013.
709 Morphology of zircon crystal grains in sediments—characteristics, classifications, definitions.
710 *Geologica Saxonica* 59, 65-73.

711 Garzanti, E., 2016. From static to dynamic provenance analysis. *Sedimentary*
712 *petrology upgraded*. *Sedimentary Geology*, 336, 3-13.

713 Giunta, A., Schmidt, D.I., Boedo, F.L., Vujovich, G.I., 2022. Análisis de procedencia
714 sedimentaria de las unidades eopaleozoicas del área del arroyo El Leoncito, Precordillera
715 Sur, provincia de San Juan. *Revista de la Asociación Geológica Argentina*, 79, 125-144.

716 Gordillo, D.E., 1996. Granitoides del sector sudeste de la Sierra de Ischilín.
717 Departamento de Ischilín-Córdoba. Tesis de Licenciatura, Universidad Nacional de Córdoba,
718 Argentina.

719 Gromet, L.P., Simpson, C., 1999. Age of the Paso del Carmen pluton and
720 implications for the duration of the Pampean Orogeny, Sierras de Córdoba, Argentina. XIV
721 Congreso Geológico Argentino, Salta, Argentina: Salta, Argentina, Actas 1, 149-151.

722 Hauser, N., Matteini, M., Pimentel, M.M., Omarini, R., 2008. Petrology and LA-ICPMS
723 U-Pb geochronology of volcanic rocks of the Lower Paleozoic rock units of the Central
724 Andes, NW Argentina: Implications for the evolution of Western Gondwana. In: VI South
725 American Symposium on Isotope Geology, San Carlos de Bariloche, Argentina, Abstracts,
726 86.

727 Hauser, N., Matteini, M., Omarini, R.H., Pimentel, M.M., 2011. Combined U-Pb and
728 Lu-Hf isotope data on turbidites of the Paleozoic basement of NW Argentina and petrology
729 of associated igneous rocks: Implications for the tectonic evolution of western Gondwana
730 between 560 and 460 Ma. *Gondwana Research*, 19, 100-127.

- 731 Heim, A., 1952. Estudios tectónicos en la Precordillera de San Juan. Los ríos San
732 Juan, Jáchal y Huaco. *Revista de la Asociación Geológica Argentina*, 7, 11-70.
- 733 Hongn, F.D., Tubía, J.M., Aranguren, A., Vegas, N., Mon, R., Dunning, G.R., 2010.
734 Magmatism coeval with lower Paleozoic shelf basins in NW-Argentina (Tastil batholith):
735 constraints on current stratigraphic and tectonic interpretations. *Journal of South American*
736 *Earth Sciences*, 29, 289-305.
- 737 Iannizzotto, N.F., Rapela, C.W., Baldo, E.G., Galindo, C., Fanning, C.M., Pankhurst,
738 R.J., 2013. The Sierra Norte-Ambargasta batholith: Late Ediacaran–Early Cambrian
739 magmatism associated with Pampean transpressional tectonics. *Journal of South American*
740 *Earth Sciences*, 42, 127-143.
- 741 Ingersoll, R.V., Bullard, T.F., Ford, R.L., Grimm, J.P., Pickle, J.D., Sares, S.W., 1984.
742 The effect of grain size on detrital modes: a test of the Gazzi-Dickinson point-counting
743 method. *Journal of Sedimentary Research* 54, 103-116.
- 744 Kay, S.M., Orrell, S., Abbruzzi, J.M., 1996. Zircon and whole rock Nd-Pb isotopic
745 evidence for a Grenville age and a Laurentian origin for the basement of the Precordillera in
746 Argentina. *The Journal of Geology*, 104, 637-648.
- 747 Keller, M., 1999. Argentine Precordillera: Sedimentary and plate tectonic history of a
748 Laurentian crustal fragment in South America. Geological Society of America. Special paper,
749 341, 131 pp.
- 750 Kury, W., 1993. Características composicionales de la Formación Villavicencio,
751 Devónico Precordillera de Mendoza. XII Congreso Geológico Argentino y II Congreso de
752 Exploración de Hidrocarburos Actas 1, 321-328.
- 753 Lenz, A., Cuerda, A., Peralta, S., 2003. Graptolites from the upper Llandovery of the
754 Talacasto area, central Precordillera, San Juan, Argentina. *Journal of Paleontology*, 77,
755 1198-1202.
- 756 Lira, R., Poklepovic, M.F., O’Leary, M.S., 2014. El magmatismo cámbrico en el
757 batolito de Sierra Norte-Ambargasta. En *Geología y Recursos Naturales de la Provincia de*

- 758 Córdoba. Asociación Geológica Argentina, XIX Congreso Geológico Argentino. Actas 1,183-
759 216.
- 760 Loske, W.P., 1992. Sedimentologie, Herkunft und geotektonische Entwicklung
761 paläozoischer Gesteine der Präkordillere West-Argentiniens. Münch Geologische Hefte 7,1-
762 155.
- 763 Loske, W.P., 1994. The West-Argentine Precordillera: a Palaeozoic back arc basin.
764 Zentralblatt Dt. Geologie Ges., 145, 379-391.
- 765 Loske, W.P., 1995. 1.1 Ga old zircons in W Argentina: implications for sedimentary
766 provenance in the Palaeozoic of Western Gondwana. Neues Jahrbuch für Geologie und
767 Paläontologie-Monatshefte, 51-64.
- 768 Lucassen, F., Becchio, R., Franz, G., 2011. The Early Palaeozoic high-grade
769 metamorphism at the active continental margin of West Gondwana in the Andes (NW
770 Argentina/N Chile). International Journal of Earth Sciences,100, 445-463.
- 771 Ludwig, K.A., 2008. User's manual for Isoplot 3.7: A geochronological Toolkit for
772 Microsoft Excel: Berkeley Geochronology Center Special Publication 4, Berkeley.
- 773 Martin, E.L., Collins, W.J., Spencer, C.J., 2020. Laurentian origin of the Cuyania
774 suspect terrane, western Argentina, confirmed by Hf isotopes in zircon. GSA Bulletin, 132,
775 273-290.
- 776 Martina, F., Astini, R.A., Becker, T.P., Thomas, W.A., 2005. The northern boundary of
777 the Precordillera terrane. Gondwana, 12, 246.
- 778 McDonough, M.R., Ramos, V.A., Isachsen, C.E., Bowring, S.A., Vujovich, G.I., 1993.
779 Edades preliminares de circones del basamento de la Sierra de Pie de Palo, Sierras
780 Pampeanas Occidentales de San Juan: sus implicancias para el supercontinente
781 proterozoico de Rodinia. XII Congreso Geológico Argentino, Actas 3, 340-342.
- 782 Mitterer, T., 2001. Charakterisierung von Magmatiten und Orthogneisen des zentralen
783 Dronning Maud-Landes/Antarctica mit Hilfe geochemischer und zirkontypologischer
784 Untersuchungen. – 1 – 104, Aachen (unpublished diploma thesis RWTH Aachen).

- 785 Morata, D., Castro de Machuca, B., Previley, L., Pontoriero, S., Arancibia, G.,
786 Fanning, C.M., 2008. New evidence of grenvillian crystalline basement in the Sierra de Pie
787 de Palo, Western Sierras Pampeanas, Argentina: Geotectonic implications In: VI South
788 American Symposium on Isotope Geology, San Carlos de Bariloche, Argentina, Abstracts, 4.
- 789 Naipauer, M., Vujovich, G.I., Cingolani, C.A., McClelland, W.C., 2010. Detrital zircon
790 analysis from the Neoproterozoic–Cambrian sedimentary cover (Cuyania terrane), Sierra de
791 Pie de Palo, Argentina: Evidence of a rift and passive margin system. *Journal of South
792 American Earth Sciences*, 29, 306-326.
- 793 Oriolo, S., Oyhantçabal, P., Basei, M.A., Wemmer, K., Siegesmund, S., 2016. The
794 Nico Pérez Terrane (Uruguay): from Archean crustal growth and connections with the Congo
795 Craton to late Neoproterozoic accretion to the Río de la Plata Craton. *Precambrian
796 Research*, 280, 147-160.
- 797 Ortiz, A., Zambrano, J.J., 1981. La provincia geológica Precordillera oriental. IIX
798 Congreso Geológico Argentino, 59-74.,
- 799 Ortiz, A., Hauser, N., Becchio, R., Suzaño, N., Nieves, A., Sola, A., Reimold, W.,
800 2017. Zircon U-Pb ages and Hf isotopes for the Diablillos intrusive complex, southern Puna,
801 Argentina: crustal evolution of the lower Paleozoic Orogen, southwestern Gondwana margin.
802 *Journal of South American Earth Sciences*, 80, 316-339.
- 803 Pankhurst, R.J., Rapela, C.W., Saavedra, J., Baldo, E., Dahlquist, J., Pascua, I.,
804 Fanning, C.M., 1998. The Famatinian magmatic arc in the central Sierras Pampeanas: an
805 Early to Mid-Ordovician continental arc on the Gondwana margin. Geological Society,
806 London, Special Publications, 142, 343-367.
- 807 Pankhurst, R.J., Rapela, C.W., 1998. The proto-Andean margin of Gondwana: an
808 introduction. Geological Society, London, Special Publications, 142, 1-9.
- 809 Pankhurst, R.J., Rapela, C.W., Fanning, C.M., 2000. Age and origin of coeval TTG, I-
810 and S-type granites in the Famatinian belt of NW Argentina. *Earth and Environmental
811 Science Transactions of the Royal Society of Edinburgh*, 91, 151-168.

- 812 Pankhurst, R.J., Rapela, C.W., Galindo, C., Alasino, P., Fanning, M., Saavedra, J.,
813 Baldo, E.G., 2008. New SHRIMP U-Pb data from the Famatina Complex: constraining Early–
814 mid Ordovician famatinian magmatism in the Sierras Pampeanas, Argentina. *Geologica*
815 *Acta*, 319-333.
- 816 Pupin, J.P., 1980. Zircon and granite petrology. *Contributions to mineralogy and*
817 *petrology*, 73, 207-220.
- 818 Ramos, V.A., Jordan, T.E., Allmendinger, R.W., Mpodozis, C., Kay, S.M., Cortés,
819 J.M., Palma, M., 1986. Paleozoic terranes of the central Argentine-Chilean Andes. *Tectonics*,
820 5, 855-880.
- 821 Ramos, V.A., Escayola, M., Leal, P., Pimentel, M.M., Santos, J.O., 2015. The late
822 stages of the Pampean Orogeny, Córdoba (Argentina): Evidence of post-collisional Early
823 Cambrian slab break-off magmatism. *Journal of South American Earth Sciences*, 64, 351-
824 364.
- 825 Rapela, C.W., Pankhurst, R.J., Casquet, C., Baldo, E., Saavedra, J., Galindo, C.,
826 1998. Early evolution of the Proto-Andean margin of South America. *Geology*, 26, 707-710.
- 827 Rapela, C.W., Pankhurst, R.J., Casquet, C., Baldo, E., Galindo, C., Fanning, C.M.,
828 Dahlquist, J.M., 2010. The Western Sierras Pampeanas: Protracted Grenville-age history
829 (1330–1030 Ma) of intra-oceanic arcs, subduction–accretion at continental-edge and AMCG
830 intraplate magmatism. *Journal of South American Earth Sciences*, 29, 105-127.
- 831 Rapela, C.W., Verdecchia, S.O., Casquet, C., Pankhurst, R.J., Baldo, E.G., Galindo,
832 C., Fanning, C.M., 2016. Identifying Laurentian and SW Gondwana sources in the
833 Neoproterozoic to Early Paleozoic metasedimentary rocks of the Sierras Pampeanas:
834 Paleogeographic and tectonic implications. *Gondwana Research*, 32, 193-212.
- 835 Sánchez, T.M., Waisfeld, B., Benedetto, J.L., 1991. Lithofacies, taphonomy, and
836 brachiopod assemblages in the Silurian of western Argentina: a review of Malvinokaffric
837 Realm communities. *Journal of South American Earth Sciences*, 4, 307-329.
- 838 Santos, J.O., Chernicoff, C.J., Zappettini, E.O., McNaughton, N.J., Greau, Y., 2017.
839 U-Pb geochronology of Martín García, Sola, and Dos Hermanas Islands (Argentina and

840 Uruguay): Unveiling Rhyacian, Statherian, Ectasian, and Stenian of a forgotten area of the
841 Río de la Plata craton. *Journal of South American Earth Sciences*, 80, 207-228.

842 Schneiderhöhn, P., 1954. Eine vergleichende Studie über Methoden zur quantitativen
843 Bestimmung von Abrundung und Form an Sandkörnern (Im Hinblick auf die Verwendbarkeit
844 an Dünnschliffen). *Heidelberger Beiträge zur Mineralogie und Petrographie*, 4, 172-191.

845 Sims, J.P., Ireland, T.R., Camacho, A., Lyons, P., Pieters, P.E., Skirrow, R.G., Miró,
846 R., 1998. U-Pb, Th-Pb and Ar-Ar geochronology from the southern Sierras Pampeanas,
847 Argentina: implications for the Palaeozoic tectonic evolution of the western Gondwana
848 margin. *Geological Society, London, Special Publications*, 142, 259-281.

849 Stacey, J.S., Kramers, J.D., 1975. Approximation of terrestrial lead isotope evolution
850 by a two-stage model. *Earth and Planetary Science Letters*, 26, 207-221.

851 Tibaldi, A.M., Otamendi, J.E., Gromet, L.P., Demichelis, A.H., 2008. Suya Taco and
852 Sol de Mayo mafic complexes from eastern Sierras Pampeanas, Argentina: Evidence for the
853 emplacement of primitive OIB-like magmas into deep crustal levels at a late stage of the
854 Pampean orogeny. *Journal of South American Earth Sciences*, 26, 172-187.

855 Thomas, W.A., Tucker, R.D., Astini, R.A., Denison, R.E., 2012. Ages of pre-rift
856 basement and synrift rocks along the conjugate rift and transform margins of the Argentine
857 Precordillera and Laurentia. *Geosphere*, 8, 1366-1383.

858 Varela, R., Basei, M.A.S., Sato, A.M., Siga Júnior, O., González, P.D., Campos Neto,
859 M.D.C., Cingolani, C.A., 2008. New U-Pb data for sierra de Umango, andean foreland at 29°
860 S, and geodynamic implications. In *Proceedings. In: VI South American Symposium on*
861 *Isotope Geology, San Carlos de Bariloche, Argentina, Abstracts*, 8.

862 Varela, R., Basei, M.A., González, P.D., Sato, A.M., Naipauer, M., Campos Neto, M.,
863 Meira, V.T., 2011. Accretion of Grenvillian terranes to the south-western border of the Río de
864 la Plata craton, western Argentina. *International Journal of Earth Sciences*, 100, 243-272.

865 Vujovich, G.I., van Staal, C.R., Davis, W., 2004. Age constraints on the tectonic
866 evolution and provenance of the Pie de Palo Complex, Cuyania composite terrane, and the

867 Famatinian Orogeny in the Sierra de Pie de Palo, San Juan, Argentina. *Gondwana*
868 *Research*, 7, 1041-1056.

869 Wenger, F.D., Arnol, J.A., Uriz, N.J., Cingolani, C.A., Abre, P., Stipp Basei, M.A.,
870 (under review) Multiproxy provenance analyses in the Devonian Villavicencio Formation of
871 the Mendoza Precordillera, Argentina: correlation and geotectonic implications in the SW
872 Gondwana margin. *Journal of Sedimentary Research*.

873 Yang, J.H., Wu, F.Y., Wilde, S.A., Xie, L.W., Yang, Y.H., Liu, X.M., 2007. Tracing
874 magma mixing in granite genesis: in situ U–Pb dating and Hf-isotope analysis of zircons.
875 *Contributions to Mineralogy and Petrology*, 153, 177-190.

876 Zimmermann, U., Bahlburg, H., Mezger, K., Berndt, J., Kay, S.M., 2014. Origin and
877 age of ultramafic rocks and gabbros in the southern Puna of Argentina: an alleged
878 Ordovician suture revisited. *International Journal of Earth Sciences*, 103, 1023-1036.

Sample	Latitud	Longitud	Methodology
16LE12	30°17'49.69"S	68°46'21.49"W	Petrography
16LE13	30°17'49.26"S	68°46'18.76"W	Petrography
16LE22	30°15'30.84"S	68°56'14.79"W	Petrography
16LE25	30°15'35.42"S	68°56'9.32"W	Petrography
16LE26	30°13'11.96"S	68°55'15.77"W	Petrography
16LE29	30°12'35.25"S	68°53'7.95"W	Petrography, Zr morphology, U-Pb and Lu-Hf

Journal Pre-proof

Sample	Latitud	Longitud	Methodology
16LE12	30°17'49.69"S	68°46'21.49"W	Petrography
16LE13	30°17'49.26"S	68°46'18.76"W	Petrography
16LE22	30°15'30.84"S	68°56'14.79"W	Petrography
16LE25	30°15'35.42"S	68°56'9.32"W	Petrography
16LE26	30°13'11.96"S	68°55'15.77"W	Petrography
16LE29	30°12'35.25"S	68°53'7.95"W	Petrography, Zr morphology, U-Pb and Lu-Hf

Journal Pre-proof

Formation	Los Espejos	Tambolar	Talacasto					Punta Negra					
Samples	16LE29	17CAR	17T04	16T40	16T45	16T63	16T64	17PN07	16PN33	16PN43	16PN59	16PN61	16PN66
16LE29		0.215	0.459	0.941	0.727	0.001	0.019	0.007	0.014	0.000	0.000	0.000	0.000
17CAR	0.215		0.011	0.898	0.700	0.002	0.001	0.155	0.088	0.000	0.000	0.000	0.000
17T04	0.459	0.011		0.789	0.159	0.000	0.109	0.002	0.001	0.000	0.000	0.000	0.000
16T40	0.941	0.898	0.789		0.846	0.313	0.163	0.327	0.182	0.000	0.000	0.000	0.001
16T45	0.727	0.700	0.159	0.846		0.000	0.003	0.069	0.036	0.000	0.000	0.000	0.000
16T63	0.001	0.002	0.000	0.313	0.000		0.049	0.000	0.001	0.000	0.000	0.000	0.000
16T64	0.019	0.001	0.109	0.163	0.003	0.049		0.000	0.000	0.000	0.000	0.000	0.000
17PN07	0.007	0.155	0.002	0.327	0.069	0.000	0.000		0.027	0.000	0.000	0.002	0.003
16PN33	0.014	0.088	0.001	0.182	0.036	0.001	0.000	0.027		0.000	0.000	0.000	0.000
16PN43	0.000	0.000	0.000	0.000	0.000	0.000	0.000	0.000	0.000		0.788	0.488	0.000
16PN59	0.000	0.000	0.000	0.000	0.000	0.000	0.000	0.000	0.000	0.788		0.694	0.003
16PN61	0.000	0.000	0.000	0.000	0.000	0.000	0.000	0.002	0.000	0.488	0.694		0.015
16PN66	0.000	0.000	0.000	0.001	0.000	0.000	0.000	0.003	0.000	0.000	0.003	0.015	

- The Los Espejos Fm evidences multiple cycles of erosion-transport-sedimentation.
- The Pampean-Brasiliano orogen represents the main source of sediments.
- The provenance proxies indicate a connection between the Jáchal and San Juan Rivers depocenters.
- The main sources of sediments are the Western and Eastern Pampean Ranges.

Journal Pre-proof

Declaration of interests

None

Journal Pre-proof